

Evaluation and Rehabilitation of Damaged Beams in Bridges

by

Salah A. Hameed

A Thesis submitted to the

Graduate School – New Brunswick

Rutgers, the State University of New Jersey

In partial fulfillment of the requirements

For the degree of

Master of Science

Graduate Program in Civil and Environmental Engineering

Written under the direction of

Professor P. N. Balaguru

And approved by

New Brunswick, New Jersey

October, 2016

Abstract of the Thesis

Evaluation and Rehabilitation of Damaged Beams in Bridges

By: SALAH AKRAM HAMEED

Thesis Director:

Dr. P.N. Balaguru

Aging infrastructures provide challenges in the areas of estimating the capacity of partially deteriorated structural members and their Rehabilitation to restore their load carrying capacity. Results presented in this thesis deals with assessing a deteriorated prestressed girder of a bridge and a procedure to strengthen the weakened beam using Fiber Reinforced Polymer (FRP) composites.

The condition of the prestressed box beam was assessed using load tests. The 46ft span beam was part of a support system containing of 21 box girders. The test-load truck was positioned to produce maximum possible moment on the deteriorated girder. All the box girders were instrumented to measure maximum tensile strain at the bottom surface of the beam. The strains at various girders were used to determine the fraction of road carried by the deteriorated girder. Stresses and strains were computed analytically for the test load and there is a good correlation between measured and computed values.

The second aspect of the thesis was to formulate a procedure to strengthen the beam using FRP composites. A fraction of the pre-tensioned wire were corroded and exposed due to environmental degradation. Carbon Fiber FRP composition repair scheme

was designed assuming zero contribution from the damaged prestressing wires and assuming complete prestress loss.

In the first scenario, amount of FRP needed to replace both prestressing force and reinforcement capacity of the damaged wire. In the second scenario, the damaged prestressing wires were assumed to act as non-prestressed reinforcement.

The results show that load testing provides an excellent tool for assessing damaged beams and FRP system can be effectively used to restore the capacity of damaged beams. Commercially available FRP systems were used for obtaining the necessary parameters for design.

ACKNOWLEDGEMENTS

I would like to take chance to express my deep gratitude to all my teachers for their guidance and consultation and to my colleagues and friends for their friendship. Special thanks are addressed to the following for their invaluable assistance in the completion of this work:

- To my advisor, Professor P.N. Balaguru, for his wisdom and guidance throughout my education at Rutgers University.
- To Professor Husam Najm, for his support during the program and my research.
- To CAIT (Center for Advanced Infrastructure and Transportation) for the Research Assistant appointments during my studies.
- To my colleague, Alaa Abd Ali, for his help and support during different phases of the research, study, and for his friendship.

Finally, I would like to express my gratitude to my wife Hiba Al-Adhami, for her support and help during all phases of my study.

Table of Contents

Abstract of the Thesis	ii
ACKNOWLEDGEMENTS.....	iv
List of Tables	vii
List of Figures	viii
Chapter One.....	1
Introduction	1
1.1 Objective of the study.....	3
Chapter Two.....	4
State of the art	4
Chapter Three	11
Research Program.....	11
Chapter Four	13
Field Testing.....	13
4.1 Description of the Test Bridge	13
4.2.1 Gage Location:	16
4.2.3 Sensors:.....	18
4.2.4 Data acquisition system and setup.....	20
A. CR6 Data logger	22
B. CDM-VW305 Dynamic Vibrating Wire Measurements.....	23
C. 12V Battery and CH200 regulator:.....	24
D. Laptop with LoggerNet software Program:	25
4.3 Test set up:.....	26
4.4 Field Test:.....	29
Installation and Field setup.....	29
Test Vehicle:.....	31
4.5 Result of live load test.....	32
Chapter Five	37

Analytical Competitions	37
5.1 Load (sharing) distribution among beams and beam properties	37
5.2. A. Maximum Absolut Moment.....	41
5.2. B. Another Approach to find M:.....	43
5.3.1 Influence of Asphalt layer on Distribution of load among the girder	45
In this part, the influence of the thickness of the asphalt layer on the concrete deck has been included:	45
5.3.2 Prestress force from the bottom strand	46
5.3.3 Fixed end moment	47
Chapter Six	49
Study for alternative solution for the bridge	49
6.1 Introduction:	49
Chapter Seven	85
Design of Repair System for Damaged Prestressed Girders Using Fiber Reinforced Polymer (FRP)	85
7.1 Background	85
7.2 Summary of Proposed Repair	87
7.3 Initial repair using epoxy mortar and surface preparation.....	88
7.4 FRP Repair design.....	88
7.5. A. Repair design calculation	90
Non-linear analysis:.....	92
7.5. B. Repair design calculation	94
Chapter Eight	95
CONCLUSIONS.....	95
REFERENCES.....	97

List of Tables

Table 3.1 - Pre-stressed properties.....	13
Table 3.2 - Location and Number of Sensors.....	16
Table 3.3a - Data for strain and displacement – Span 1.....	31
Table 3.3b - Data for strain and displacement – Span 2.....	33
Table 6.1 - AASHTO girder section properties	51

List of Figures

Figure 4.1 - Bridge side view	14
Figure 4.2 - Structure No. 1223-153, Route 35	14
Figure 4.3 - Bridge's top view	15
Figure 4.4 - Locations of Sensors	17
Figure 4.5 - Vibrating wire strain gauge (4000)	19
Figure 4.6 - 8510 Potentiometer	20
Figure 4.7 - Data Acquisition Diagram	21
Figure 4.8 - Data Acquisition System during Monitoring	21
Figure 4.9 - Campbell Science CR6 Data	22
Figure 4.10 - CDM-VW305 Dynamic Vibrating	23
Figure 4.11 - 12V Battery and CH200	24
Figure 4.12 - LoggerNet computer program	25
Figure 4.13 - Strain gage and PT Flexure Testing	27
Figure 4.14 - Strain gauge and PT8510 Transducer / Flexure Testing	28
Sample Testing Concrete Blocks	
Figure 4.15 - Installed 4000 Vibrating wire strain Gauges	29

Figure 4.16 - Installed 4000 Vibrating wire strain Gauges and PT 8510	30
Figure 4.17 - The weights and distances for the load vehicle	31
Figure 4.18 - Strain gauges scrawling for Beams 3, 4, 5, and 6	36
Figure 5.1 - Strains along the cross section of the bridge	38
Figure 5.2 - Bottom bars	39
Figure 5.3 - Top bars	39
Figure 5.4 - cross section in box-girder	39
Figure 5.5 - The relation between the distribution factor and strain.....	41
Figure 5.6 - vehicle test location on the bridge	41
Figure 5.7 - SFD and BMD for the beam	44
Figure 5.8 - cross section in box-girder with bottom reinforcement	44
Figure 5.9 - The relation between the Asphalt's Modulus of elasticity..... and strain	46
Figure 5.10 - The relationship between the fixed end moment	48
and the strain	
Figure 6.1 - Cross section in bridge deck	50
Figure 6.2 - Girder spacing versus span length	52
Figure 6.3 - Type 4 girder	53

Figure 6.4 - Girder details	57
Figure 7.1 - Damaged Beams BM3 and BM 4 in Span 1	86
Figure 7.2 - Damaged Beams BM18 and BM19 in Span 1	86
Figure 7.3 - Damaged Beams BM3 and BM4 in Span 4	87
Figure 7.4 - Damaged Beams BM18 and BM19 in Span 4	87
Figure 7.5 - Typical detail of FRP Repair. Beam width is 36-inches.....	89
FRP width shall be 30-inches	
Figure 7.6 - calculate the maximum moment capacity using	93
non-linear approach	

Chapter One

Introduction

Continuously operating instrumented structural health monitoring (SHM) systems are becoming a practical alternative to supersede visual inspection for assessment of condition and health of civil infrastructure, such as bridges. Although, the large amount of data from an SHM system needs to be converted to useable information, it is still considered a great challenge to which special signal processing techniques must be applied. This study is devoted to the identification of abrupt, anomalous, and potentially onerous events in the time histories of static, instantaneous sampled strains recorded by a multi-sensor SHM system installed in a major bridge structure and operating continuously for three types of tests (static, dynamic, and crawling). Such events may result from, among other causes, sudden settlement of foundation, ground movement, excessive traffic load or failure of posttensioning cables.

It is much more efficient to provide in-place repair girders than to completely shut down or reroute interstate highway traffic to rebuild a bridge. An effective in-place repair is needed for these bridge girders. The pre-repair load test and a post-repair load test are required to determine the effectiveness of the FRP repair. The pre-repair load test results provide a baseline for which the post-repair load test results can be compared. The pre-repair load test will also provide information to better understand the current bridge behavior. Thus, it is important to have updated information on structural condition and performance of bridges in order to earlier detect any worrying signs of decline and undertake protective countermeasures.

In this study, the pre-repair static load test was described for a bridge in Perth Amboy, New Jersey. In the test, bridge girders were instrumented, and data was collected while a NJDOT load truck was positioned in predetermined locations along the bridge surface. The results of the tests were recorded, and the measured bridge response was examined to gain insight into the structural behavior of the system. Conclusions about the behavior of the bridge were reported, and ideas were introduced about the possible variation of bridge behavior with strain and displacement. A portion of the load test was focused on using the principle of superposition to determine whether the existing bridge superstructure behaves as a linear-elastic system under service-level loads.

One of the major challenges of a SHM study is making sense of large amounts of data that continuously operating SHM systems produce. For the success of SHM, the data needs to be reduced into manageable volumes and forms, and then that information needs to be extracted and then be developed as knowledge about structural condition. There are likely to be major differences between the relatively basic expectations and requirements of infrastructure managers and the ambitions of systems designers; the latter usually originally academic.

Transportation infrastructure authorities have long recognized the need to keep their bridges healthy and to this end have implemented various inspection and management programs. The current health monitoring practice is primarily based on visual inspection. Due to high manpower demand, such inspections cannot be performed frequently. Other drawbacks of visual inspection based condition assessment include inaccessibility of critical parts of the structure and lack of information on actual loading. These shortcomings lead to subjective and inaccurate evaluations of bridges' safety and

reliability. As a result, some bridges may be retrofitted or replaced, while in fact they are sound. On the other hand, existing damages in other bridges may not be identified until they become expensive to repair or dangerous for structural integrity.

1.1 Objective of the study

The objective of the research described in this thesis is to perform the pre-repair static load test required to determine the effectiveness of the FRP repair and analyze the results. The pre-repair test will provide a baseline to which the post-repair test can be compared. The test data is also analyzed to determine both the behavior of the cracked girders and the effectiveness of superposition.

Chapter Two

State of the art

Beginning in the late 1950's in the United States, the continuous prestressed bridges have been developments to making multi-span and connecting the ends of the girders over the supports. This began an investigation for improvement, which included the connection between the girders by diaphragm connecting. Timely in this process, the Portland Cement Association noticed that continuity could be beneficial in three different ways (Kaar, et al 1960). First, both the deflection and maximum moments at the mid span of girder could reduce by the continuity over support, also, approximately 5 to 15 percent fewer strands could be allowed to be used when using the continuous girders, and also more than this percent could be achieved (Freyermuth 1969). Second, the long term durability of a girder could be developed by eliminating the joints over the support since that will reduce the amount of water and salt, which are the main factors causing the deterioration in the concrete. Also, the riding surface could be improved by eliminating the joints. Third, the reserve load capacity in the event of an overload condition could be provided by the continuity of a girder.

On the other hand, over the past fifty years, many states have been familiar with the benefits of making precast, prestressed multi-girder bridges continuous by connecting the girders with a continuity diaphragm. Further, there has not been as much agreement on either the methods used for design of these system or details used for the continuity connection, although there is agreement on the benefits of continuous construction.

Surveys show that 21% of the bridges in the US bridge inventory are prestressed, as are more than half of the new bridges being built each year (TRB 2000).

Prestressed concrete bridges are often made of simple-span girders. The performance of these bridges can be improved by providing a positive moment connection between the girders after they are set in place. This makes the bridge simple span for structural dead loads, but continuous for all superimposed loads. In addition to a more favorable distribution of loads, these bridges have a number of practical and economic benefits, such as improved durability, elimination of bridge deck joints, and reduced maintenance costs.

The New Jersey Department of transportation (NJDOT) is currently involved in a bridge rehabilitation and replacement program where each of the state's bridges is assessed to determine its rehabilitation needs. One of the bridges identified for rehabilitation is located in Perth Amboy NJ.

Most precast, prestressed girders used for bridge construction are non-composite for self-weight and the dead load of the deck but are later made composite by the addition of a cast-in place concrete deck. Therefore, both composite and non-composite properties must be considered in the design process. Also, unique to this type of construction, the construction sequencing can have a large influence on the behavior of the system.

Once a multi-span system is made continuous, thermal restraint moments will develop and induce additional stresses in the system. Some design methods do not consider these influences; however, the stresses caused by the thermal restraint moments may be significant and have been considered in this study.

Considering just some of these influences, it can be seen that the behavior of a system made of precast, prestressed concrete made continuous can be difficult to predict. As some responses begin to influence the behavior of other material properties, the validity of using the law of superposition begins to be questioned, making the prediction of the behavior of these systems even more difficult.

Various studies have been conducted since but, except for minor modifications, the fundamental analysis methods have remained the same. Recent developments in analysis methods and material behavioral research, coupled with long-term experimental and field observations, have raised questions as to the validity of accepted analysis methodology for these bridges. Recent research has determined that the long-term behavior of ‘continuous for live load’ bridges is not predicted accurately by industry-accepted methods of analysis. Specifically, these analytical models predict an alteration in the distribution of moment in the structure, caused by shrinkage of concrete, which is not confirmed by experimental data. The greatest challenge in modeling ‘continuous for live load’ is determining a technique for simulating the complex creep and shrinkage behavior of prestressed concrete and the shrinkage and cracking behavior of reinforced concrete. A logical first step would be to model a simple span structure and be sure that the creep, shrinkage and cracking behaviors can be accurately modeled. When this is confirmed, these modeling techniques will be available for use in modeling ‘continuous for live load’ bridges. This study attempts to simulate creep due to prestress and dead load in the girders, differential shrinkage between the deck and girder and cracking in the deck of a single span bridge.

Finally, this type of construction had the following advantages over conventional simple span bridges: i) the maintenance costs associated with bridge deck joints and deck drainage onto the substructure, were reduced or eliminated. ii) Continuity improved the appearance and riding quality of the bridge. iii) Seismic performance was improved (Miller et al 2004). iv).The structural economy of a continuous design and the elimination of deck joints, guaranteed an initial economic advantage (Freyermuth 1969).

Health monitoring of civil infrastructures has achieved considerable importance in recent years, since the failure of these structures can cause immense loss of life and property. However, the large size and complex nature of the civil–structural systems render the conventional visual inspection very tedious, expensive, and sometimes unreliable, thus necessitating investigations for the development of automated techniques for this purpose. Many monitoring techniques have been reported in the literature, the most popular among the researchers in civil engineering being those based on the response of low-frequency vibration on the structures. Using these techniques, the first few mode shapes are extracted and processed to assess the locations and the amount of damage. Some of the prominent algorithms employing this principle include the change in stiffness method (Zimmerman and Kaouk 1994), the change in flexibility method (Pandey and Biswas 1994), and the damage index method (Kim, Jeong-Tae 2003). Basically, SHM should be broadly defined as “the use of insitu, nondestructive sensing and analysis of structural characteristics, including the structural response, for the purpose of identifying if damage has occurred (Level 1 of diagnostics), determining the location of damage (Level 2), estimating the severity of damage (Level 3), and evaluating

the consequences of damage on structural serviceability, reliability and durability (Level 4)” (C. Sikorsky 1999).

The development of structural health monitoring technology for surveillance, evaluation and assessment of existing or newly built bridges has now attained some degree of maturity. On-structure long-term monitoring systems have been implemented on bridges in Europe, the United States, Canada, Japan, Korea, China, and other countries. Bridge structural health monitoring systems are generally envisaged to: (i) validate design assumptions and parameters with the potential benefit of improving design specifications and guidelines for future similar structures; (ii) detect anomalies in loading and response, and possible damage/deterioration at an early stage to ensure structural and operational safety; (iii) provide real-time information for safety assessment immediately after disasters and extreme events; (iv) provide evidence and instruction for planning and prioritizing bridge inspection, rehabilitation, maintenance and repair; (v) monitor repairs and reconstruction with the view of evaluating the effectiveness of maintenance, retrofit and repair works; and (vi) obtain massive amounts of in situ data for leading-edge research in bridge engineering, such as wind- and earthquake-resistant designs, new structural types and smart material applications (Ko, J. M., and Y. Q. Ni 2005).

To date, numerous structure health monitoring methodologies and systems have been proposed, and some of them have been applied on the full-scale bridge structures: e.g., the Alamosa Canyon Bridge (Farrar, C. R., and S. W. Doebling 1997), the I-10 Bridge (Todd et al. 1999), the Hakucho Bridge in Japan (Abe et al. 2000), the Bill Emerson Memorial Bridge in Missouri (Çelebi et al. 2004), and the Tsing Ma Bridge in

Hong Kong (Wong 2004), to name a few. Though these examples demonstrated the significant potential of SHM, the cost of obtaining the relevant information for structure health monitoring on large structures is high (Rice and Spencer 2009). For example, the Bill Emerson Memorial Bridge is instrumented with 84 accelerometer channels with an average cost per channel of over \$15 K, including installation (Jang, Shinae, et al. 2010).

Continuously operating structure health monitoring systems generally produce various “raw” signals, such as displacements, accelerations, strains, stresses, temperatures, wind velocities, or signals resulting from some form of analytical processing of the raw data, e.g. natural frequencies or power spectra. Because of the character of signals recorded by structure health monitoring systems, i.e. time series sampled over long periods of time and at regular intervals, such data naturally lend themselves to examination using the extensive and proven tools offered by the time series analysis and statistical process control. The concepts of the time series analysis have successfully been applied to numerous problems, notably in the field of econometrics, where they have been used, for example, to investigate stock prices, production and prices of various commodities, and interests rates (Wei, 1993). Little has been reported, with the exception of the aforementioned study by Sohn et al. (2000), about application of time series analysis in the area of SHM of civil infrastructure. Another publication is that of Moyo and Brownjohn (2002b) who used intervention analysis for assessing the impact of various events during construction of a bridge on the recorded time series of strains. The present study uses several existing procedures of the time series analysis to understand and extract information from the strain data recorded on a bridge structure.

The main objective is to identify abrupt events sustained by the bridge and possible structural change or damage.

Chapter Three

Research Program

The concept of structural health monitoring has been the subject of research over the last few years, especially in civil and structural engineering where the major concern for the infrastructure is the old age. These studies have direct to initiatives towards the development and employment of new sensing technologies. According to the tough environments found in the construction industry, and the large size of civil engineering structures, such sensors should be strong, tough, easy to use and economical.

The result reported in this dissertation deals with:

- Lab testing for the equipment that used in the field test, this equipment should prepare and calibrate before using in the field test. Also, this equipment have attached to the concrete beam in the lab and test for the flexural test to ensure the correct reading for the sensors and data acquisition.
- Field testing of Prestress concrete girder, the test was in the site to collect the data from the girders of the bridge, and this test have done with install 21 sensors for the strain and eight sensors for displacement, and connect these sensors to data acquisition, and connect the data acquisition to the computer to collect the data.
- Analysis an actual bridge to verify the measurements and interpretation of load-test result, and analysis the data that have gotten from the bridge to compare with the standard

- Analysis for replacing the box-girder by I-section girder to avoid the damage which was happened for the girder by prevented the water from drainage. Also, the cost for I- section girder less than the box-girder.
- Analysis of damage girder and strengthened Prestress concrete girder, and recommendation for repairing the Prestress concrete girder.
- Procedure for repairing damaged girder by using FRP to avoid the bridge replacement and prevent them girder from the corrosion by the time.

A typical SHM system comprises an array of sensors, sensor warning hardware, a host computer and communication hardware and software. Sensors play the important role of providing information about the state of strain, stress and temperature of the structure. Their selection for a particular application is governed by application, sensor sensitivity, power requirements, robustness and reliability. Most SHM systems reported in the literature have focused on traditional sensing technologies such as electrical resistance strain sensors, vibrating wire strain gauges and piezoelectric accelerometers. While the traditional sensors are robust and strong enough for civil engineering applications they often require many cables to support them, and for long distance monitoring these cables suffer from electromagnetic interference (EMI).

Chapter Four

Field Testing

4.1 Description of the Test Bridge

The bridge (structure No. 1223-153) is located on NJ Route 35 over Perth Amboy Connector (NJ 440), Abandoned Perth Amboy (South Plainfield Branch) and Conrail. The bridge has four spans (3-main & 1-approach), is simply supported, is composite, is a pre-stressed concrete box beams in main span, and has voided slab beams in the south approach span. This bridge was built in 1960 and underwent rehabilitation in 1972. The rehabilitation repaired the spalls in pre-stressed beams with exposed strands in Spans 1 and 4. Cracks in the pavement on the approach roadway and over the abutment deck joints have been partially sealed. The bridge is in serious condition due to the superstructure. The bridge consists of 21 adjacent 3'-0" wide x 2'-3" high x 236' long pre-stressed concrete beams and an average 5.5" thick composite concrete deck. On each side of exterior concrete girder, curbs and guardrails are located. The annual average daily traffic was 22,300 vehicles and truck ADT is 4% in 2004 for this bridge. For testing, a 58,000 lb 3-axle truck was driven over the bridge. All 21 concrete beams were pre-stressed to have the properties in Table 4.1:

Table 4.1 Pre-stressed properties

strength of, f'_c	5000 psi
Strength of, f'_{ci}	4000 psi
Pre-stressing steel yield	248,000 psi
Reinforcing steel yield	40,000 psi
pre-stressing steel	7/16 Ø uncoated
Stressed- relived seven wires strans. F_i	27,000 psi, per strand

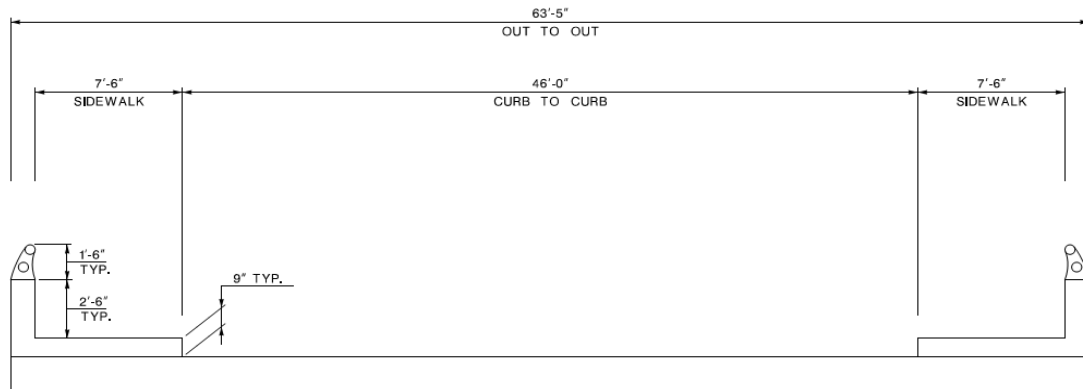


Figure 4.1 Bridge side view



Figure 4.2 - Structure No. 1223-153, Route 35

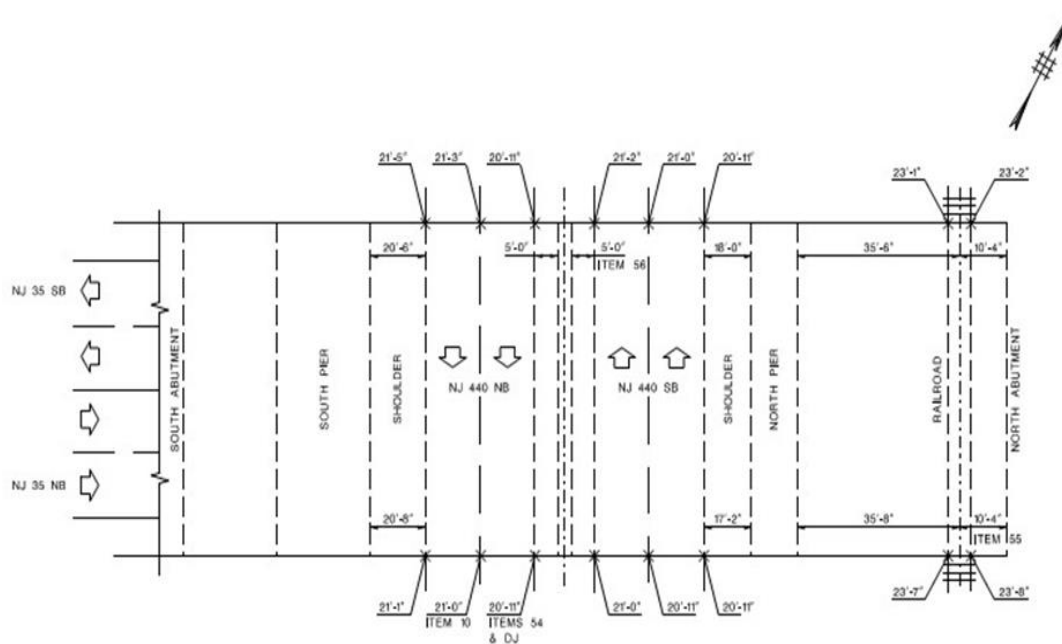


Figure 4.3 - Bridge's top view

The instruments used in this investigation have been provided by several well-known companies. The datalogger and its belongings were provided by Campbell Science, while the dynamic strain sensors were provided by Geokon. Finally the displacement potentiometers were provided by Celesco. The following will be introduced to describe details of the instruments:

- 1- Gage Location
- 2- Instrumentations
- 3- Sensors
- 4- Data acquisition system and setup

4.2.1 Gage Location:

The strain gage has been attached in the middle of the span because of the expected maximum strains in this location. There were 17 strain gages and 8 PTs installed in the bottom of the beams in the post-tension rods. In addition, 17 strain gages were attached to the bridge, one per beam. Two beams from each side did not have strain gages because of its walkway. Four PTs were also attached to four beams on each side.

Generally, these settings were chosen to discuss:

- Effects of the post-tensioning rod, especially for beam 3 and beam; these beams were damaged
- Load transfer from beam 3 and beam 4 to other beams
- The bending of the first four beams from each side, four beams chosen to compare between the first two that damaged and beams 5 and 6 respectively, to see what is the difference in displacement

Table 4.2 Location and Number of Sensors

	Strain Gage	PT
Beam 3 to Beam 19	17	
Beam 1 to beam 4		4
Beam 16 to beam 19		4

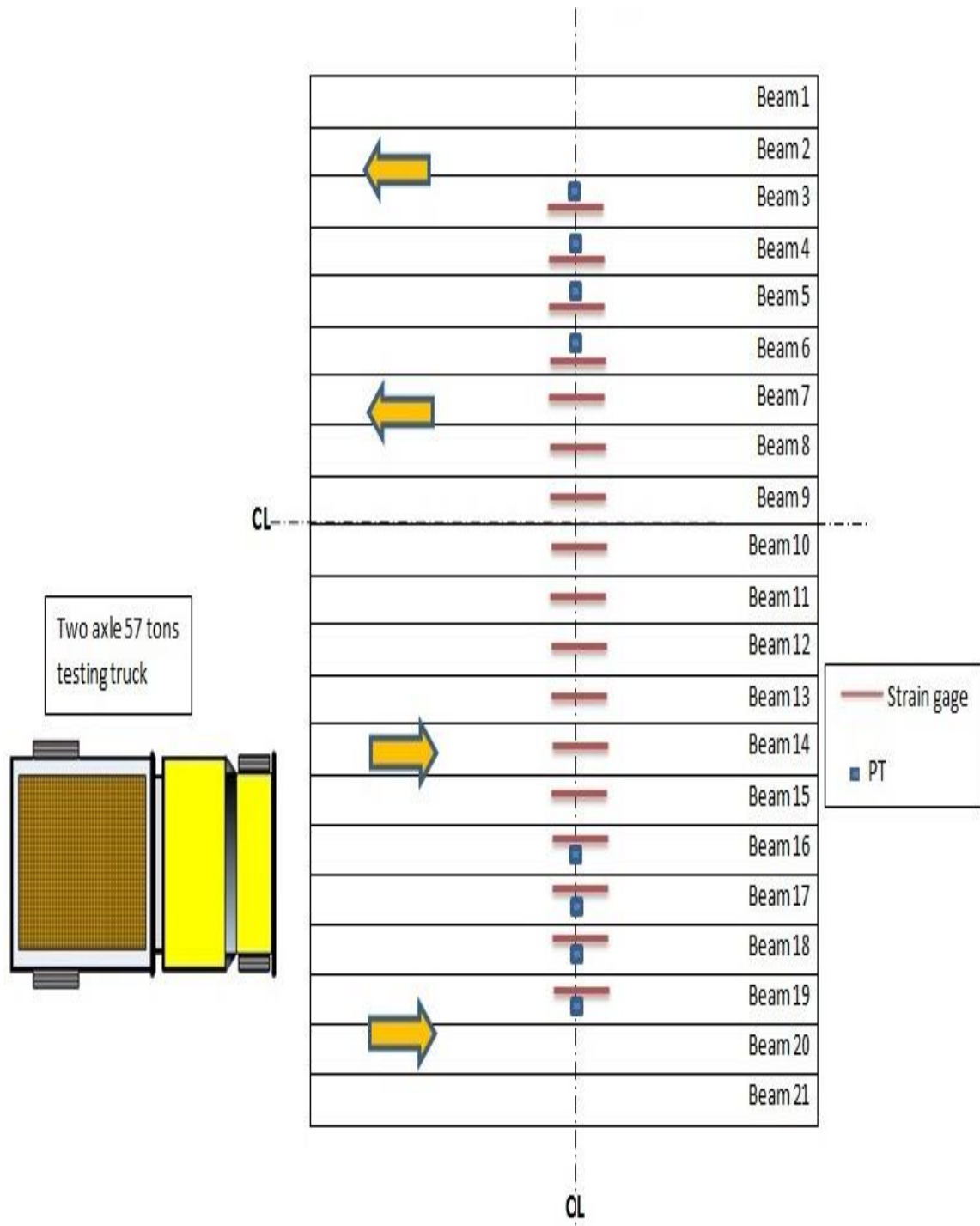


Figure 4.4 Locations of Sensors

4.2.2 Instrumentations:

The instruments that were used for this investigation were Geokon 4000A vibrating wire strain gages and Celesco 8510 displacement potentiometers. Both strain gages and PTs were attached underneath the beams of the bridge. To connect these instruments to a computer and collect data, these instruments needed a data acquisition device. The gages connected to a 16 x 18 inches enclosure; this enclosure contained a CR6 data logger, a CDM-VW305, a 12V battery, and a charger. The 4000A strain gages connected to a CDM-VW305, and the CDM-VW305 connected to a CR6. The 8510 PTs connected directly to a CR6 data logger. The CR6 data logger connected to the laptop. The CR6 data logger received power from the battery while the charger charged the battery. All other instruments in the board received power from the CR6. The lead wires connected the 8510 PTs and the strain gages to the enclosure. All connection was completed on the day of the field test. However, access under the bridge was not allowed during the day of the field test, but, NJDOT prepared all the appropriate papers to allow us access at a future time.

4.2.3 Sensors:

All strain gages' data was recorded to the CDM-VW305 then from the CDM-VW305 to the CR6 data logger. Then the PTs' data was recorded directly to the CR6 data logger. These strain gages and PTs attached directly to the bottom of the beams for the bridge by using the instant adhesive glue. The installation of the gages was done by three research assistants from Rutgers the State University of New Jersey. Two types of instruments were used in this investigation:

- 1- The Geokon model 4000 vibrating wire strain gage, is intended primarily for long-term or short-term strain measurement on any steel or concrete structure such as tunnel lining, arches, struts, piles, bridges, sheet pilings, etc. The strain gage uses the vibrating wire principle: a length of steel wire is tensioned between two mounting blocks that are attached to a concrete beam. Deformations of the surface causes the two mounting blocks to move relative to one another, thus altering the tension in the steel wire. The tension in the wire is measured by plucking the wire and measuring its resonant frequency of vibrating. The wire is plucked, and its resonant frequency measured, by means of an electromagnetic coil positioned next to the wire. See Figure 4.5 (Manual from Geokon Inc. 2014)

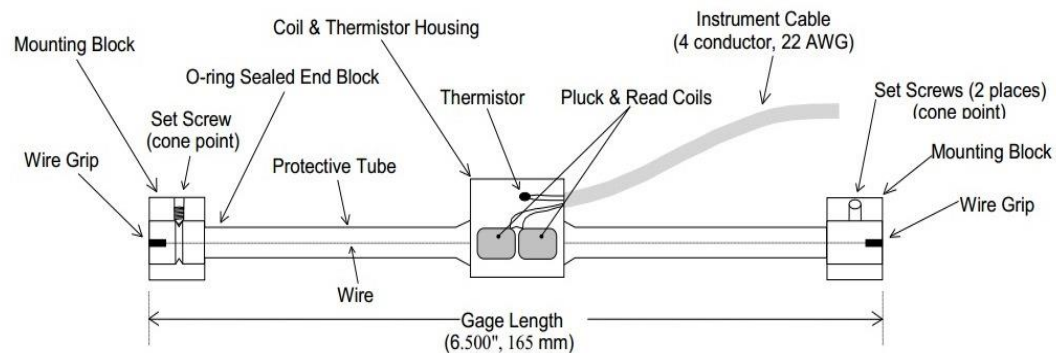


Figure 4.5 Vibrating wire strain gauge (4000)

- 2- The Celesco PT 8510 displacement potentiometer, detects and measures linear position and velocity using a flexible cable made from stainless steel and a spring-loaded spool with an optical encoder sensor. The cable measurement for the model that was used in this investigation was ranging

between (0 – 6 inches). This model is designed for rough environments, injecting modeling, and detecting the linear displacement for structures from the gravity load. The accuracy of this model is 0.04 % from the full stroke. The total weight of the sensor is 3 lb.

To ensure the compatibility between the PT 8150 and the CR6 there is a special setup that should be provided for the PT 8150. The input voltage for the PT 8150 should range between (0 – 5 volte), the operating temperature should range between (0 – 160 F), and the maximum vibration is 10g. (See figure 4.6)

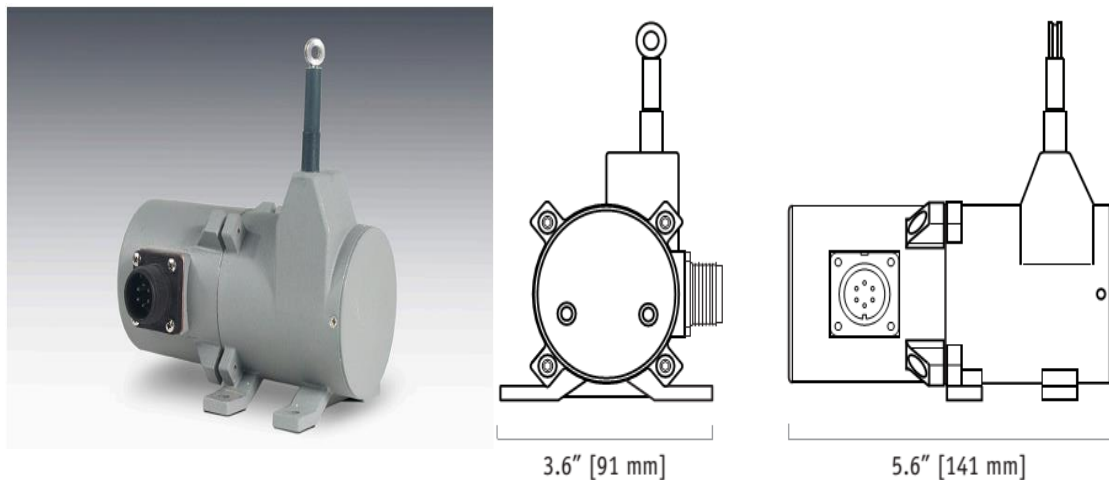


Figure 4.6 - 8510 Potentiometer

4.2.4 Data acquisition system and setup

During this investigation, the CR6 data logger was used for the control system and measurement, the CDM-VW305 connected the strain gages to the CR6 data logger, and the battery and charger gave power to the system. In addition, the CR1000 data logger, CR3000 data logger, CS-CPI data logger and AM16/32 relay multiplexers were

used in the lab work at the beginning of the investigation at the lab, but in the final setup the CR6 was satisfactory for site investigation. Further, a generator and laptop were used in this investigation. (See figure 4.7 and 4.8)

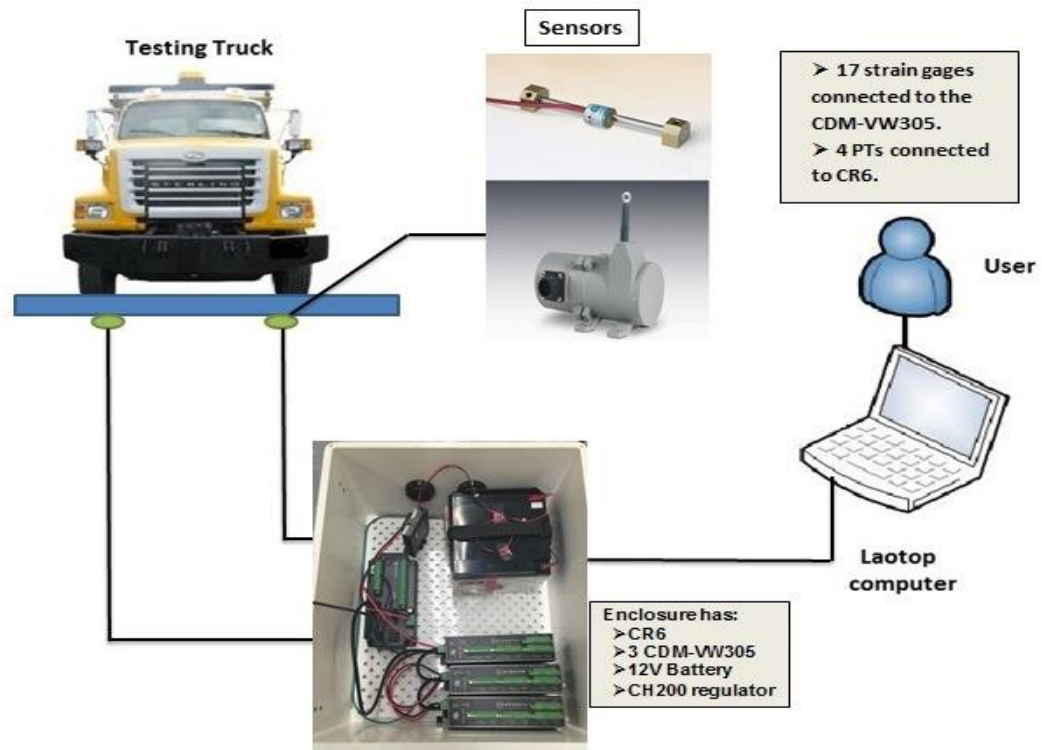


Figure 4.7 - Data Acquisition Diagram



Figure 4.8 - Data Acquisition System during Monitoring

A. CR6 Data logger

The CR6 data measurement and control system manufactured by Campbell scientific, Inc. is a powerful core component of a data-acquisition system, adding faster communications. Further, it combines the best features of all data loggers, has low power requirements (flexible power input from solar panel, DC power supply, 12V battery, or USB), has built in USB, and is a compact size. CR6-series data loggers feature universal (U) terminals, which allow connection to virtually any sensor-analog, digital, or smart, onboard communication via Ethernet 10/100. It has a micro SD card drive for extended memory requirements, support for serial sensors with RS-232 and RS-485 native, and CPI for hosting Campbell high-speed sensors and distributed modules (CDMs). It is programmable with CRBasic or SCWin program generator, completely PakBus compatible, and has a shared operating system (OS) with the popular CRBasic CR1000 and CR3000 data loggers. (Campbell Scientific, Inc.2015). (See figure 4.9)



Figure 4.9 - Campbell Science CR6 Data

B. CDM-VW305 Dynamic Vibrating Wire Measurements

The CDM-VW305 is an 8-channel link between sensors and data loggers that takes less time to gather data, and gathers the data simultaneously. This link uses an excitation mechanism that ensures the vibrating wire sensor operates in a continuously vibrating state. The interface measures the resonant frequency of the wire between excitations using the patented vibrating wire spectral-analysis technology. The CDM-VW305 provides very fine measurement resolution and also limits the effects of external noise by distinguishing between signals and noise based on frequency content. Because of this technology, signals can be carried through longer cables, providing compatibility between the sensors and the CR6 data logger. . (See figure 4.10).

The CDM-VW305 interfaces with standard vibrating wire sensors, giving much faster and more accurate. The CDM-VW305 has eight channels per module; synchronized across multiple modules. Furthermore, it has dynamic measurement rates of 20 to 333 Hz. In addition, the CDM-VW305 has low power requirements; it can work by a flexible power input from solar panel, DC power supply, or 12V battery.



Figure 4.10 - CDM-VW305 Dynamic Vibrating

C. 12V Battery and CH200 regulator:

The 12V battery supplied the power for all instruments in the enclosure and it was charging from the CH200 regulator. The 12V battery includes a 24in. attached cable that terminates in a connector for attaching the battery to a CH200 regulator. The CH200 regulator was connected directly to power source. The CH200 allows charging from various sources: solar panels, AC wall chargers, and a generator. The CH200 allows simultaneous connection of two charging sources such as solar panel and AC wall charger. The CH200 has the ability to monitor both load and battery current. (See figure 4.11).

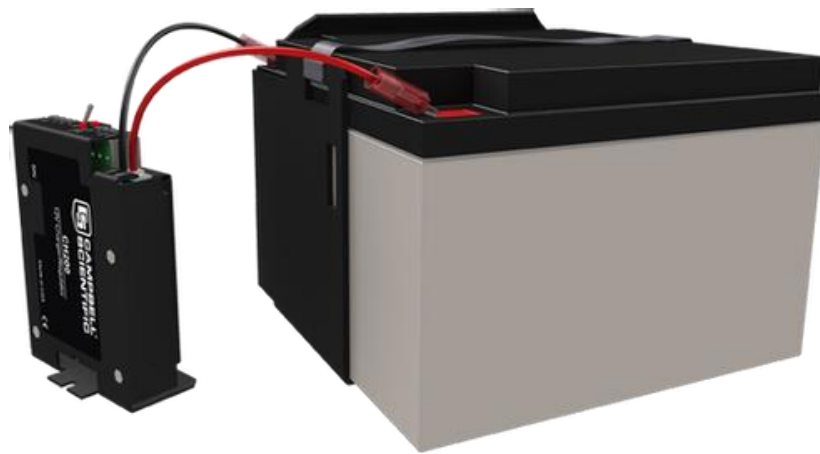


Figure 4.11 - 12V Battery and CH200

D. Laptop with LoggerNet software Program:

The CR6 data acquisition system is operated by a computer-coded program. Campbell Scientific team was helping to create a program code that is compatible with 17 strain gages, eight PTs, the CR6, and the CDM-VW305. To collect and control necessary data at the live load test, first the LoggerNet computer application had to be installed and then the conformed program code on the data acquisition laptop computers was processed. The LoggerNet software supports the CR6 program generation, real-time display of data-logger measurements, graphing, and retrieval of data files. (See figure 4.12)

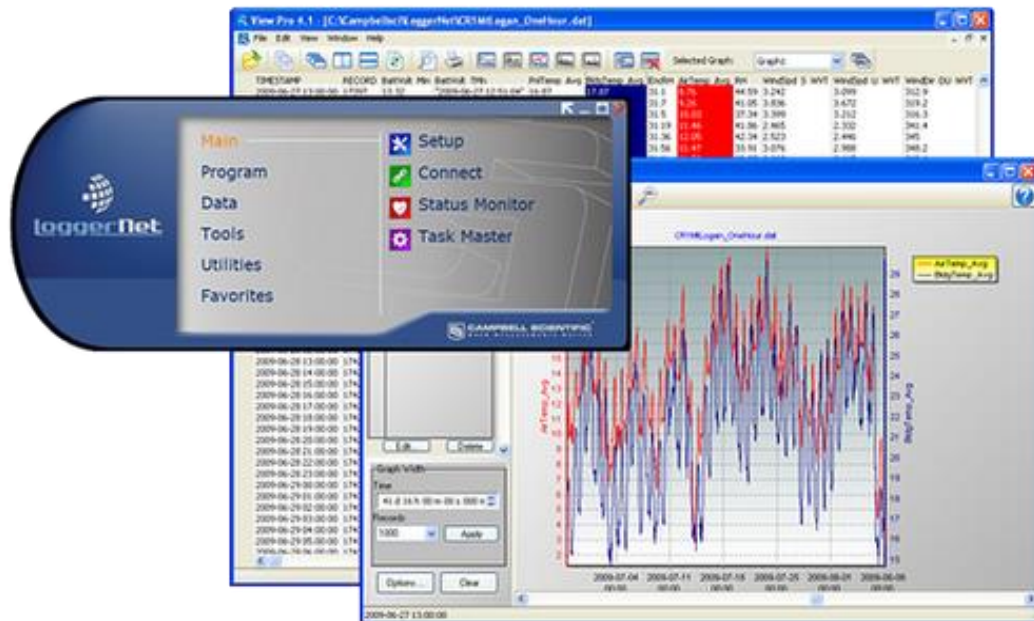


Figure 4.12 - LoggerNet computer program

4.3 Test set up:

To ensure the accuracy and performance of the field instrumentation, a lab test was performed at the Civil Engineering Laboratory at Rutgers University. In addition, it was necessary to check the field procedure, and then compare those results with the results from the lab test.

One concrete beam sample was prepared and tested in the lab. The beam made of plain concrete according to C192, and the cross sectional dimension of the concrete beam were 6 x 6 inches and the total length was 20 inches, while the clear span was 18 inches. Compressive strength of cylindrical concrete specimens had been tested according to C39. The average compressive strength of the cylinders was 6250 psi. According to ACI318, the modulus of rupture was given by:

$$f_r = 7.5 f'_c$$

In this lab test, it was found that flexural strength was 593 psi.

The test setup was designed for 50% of the flexural strength. For that, the maximum flexural strength in the lab test had not exceeded 300 psi to avoid the brittle failure of plain concrete. See Figure (4.13).

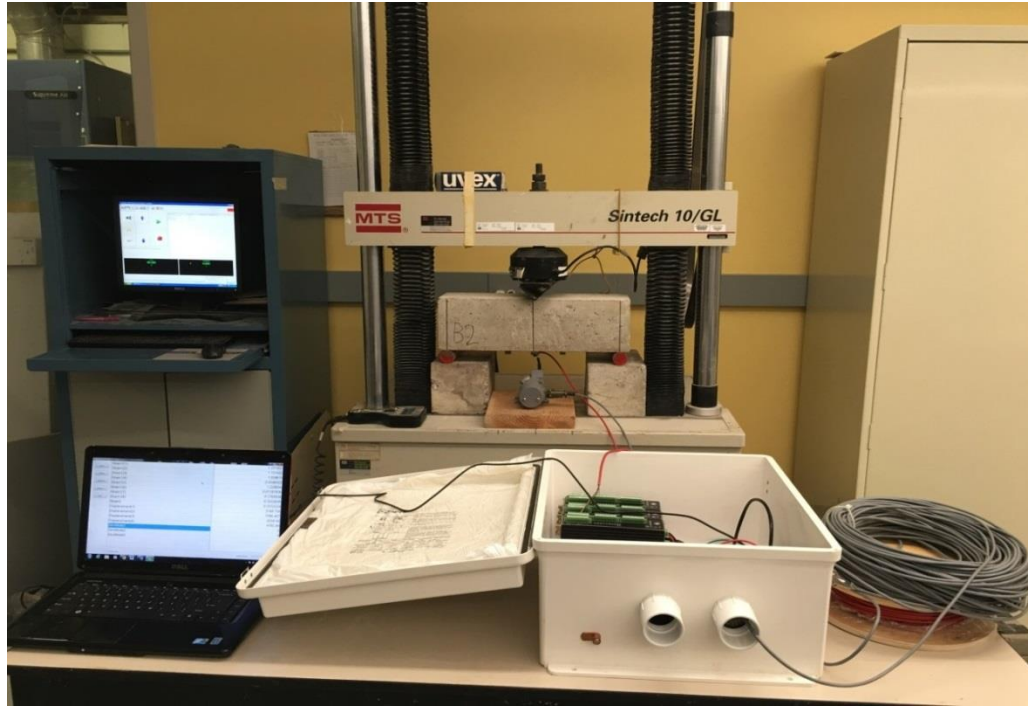


Figure 4.13 - Strain gage and PT Flexure Testing

The strain gage and PT were attached on the bottom side of the experimental concrete beam. Figure 4.14 shows the concrete beam with sensors attached in the lab. Before the test, the 16 x 18 in. enclosure, with the CR6 data logger and the CDM-VW305, were prepared and connected with the sensors for the test. The MTS Sintech 10/GL testing machine was used for three point flexure test. The applied total load was recorded and plotted by the MTS computer program. The strain and displacement were recorded by LoggerNet on the laptop computer.

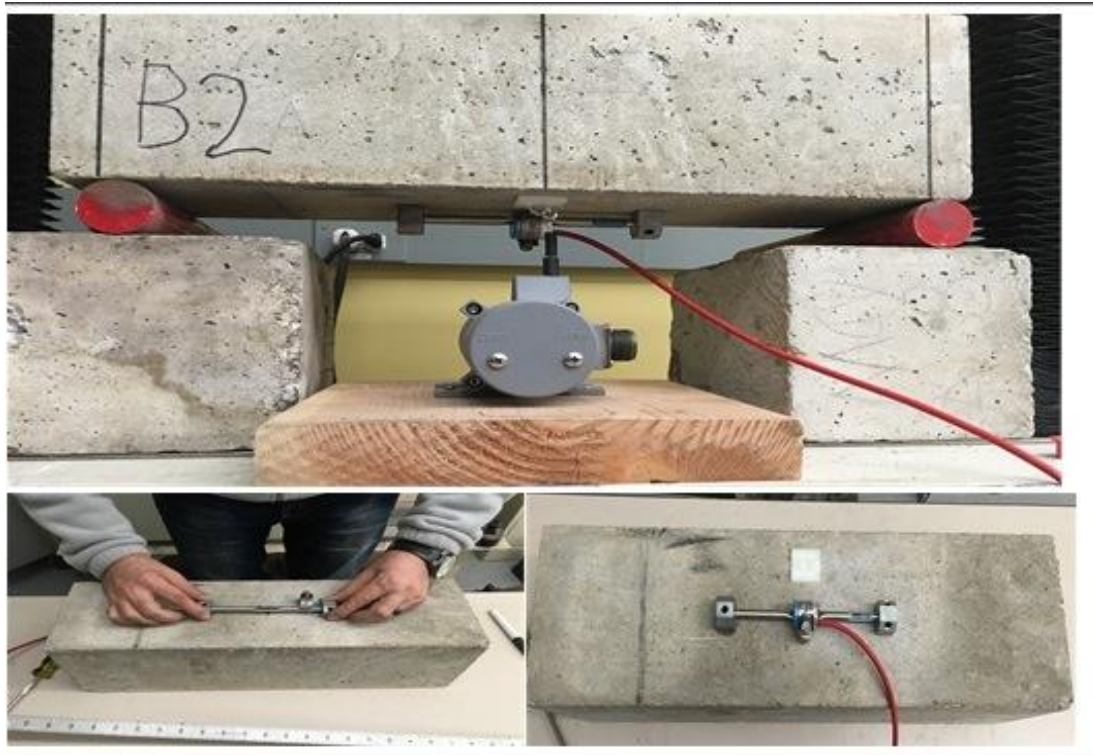


Figure 4.14 - Strain gauge and PT8510 Transducer / Flexure Testing Sample Testing Concrete Blocks

The moment of inertia of the cross section of the concrete beam was 108 in^4 , and the designed flexural strength was 300 psi, therefore, the expected applied moment was 10,800 lb.in. The MTS machine was setup to stop when the applied moment reached 10,800 lb.in, and this moment was expected to develop when the machine load reached 2400 lb.

The load was applied continuously with a deflection control until the load reached 2400 lb. with a loading rate equal to 0.05 in/min.

As a result, the reported data showed an adequate compatibility between the field instrumentation and the MTS machine with an off error less than 2%.

4.4 Field Test:

Installation and Field setup

In advance, the sensors were attached to the bridge by the research team on the first week of December, 2015. The boom lift truck was used to reach the bottom of the bridge to attach the sensors. The lead wire was used to connect the sensors to the enclosure, all 17 strain gages were connected to the CDM-VW305 and 8 PTs were connected to the CR6 data logger correctly. The connection was checked by each sensor's specific resistance value using the multi-meter. The State of New Jersey Department of Transportation (NJDOT) and the Center for Advance of Infrastructure and Transportation (CAIT) provided access to the site. The traffic arrangement and the loading test vehicle supplied were by the Maintenance of Traffic (MOT). (See figure 4.15 and 4.16)

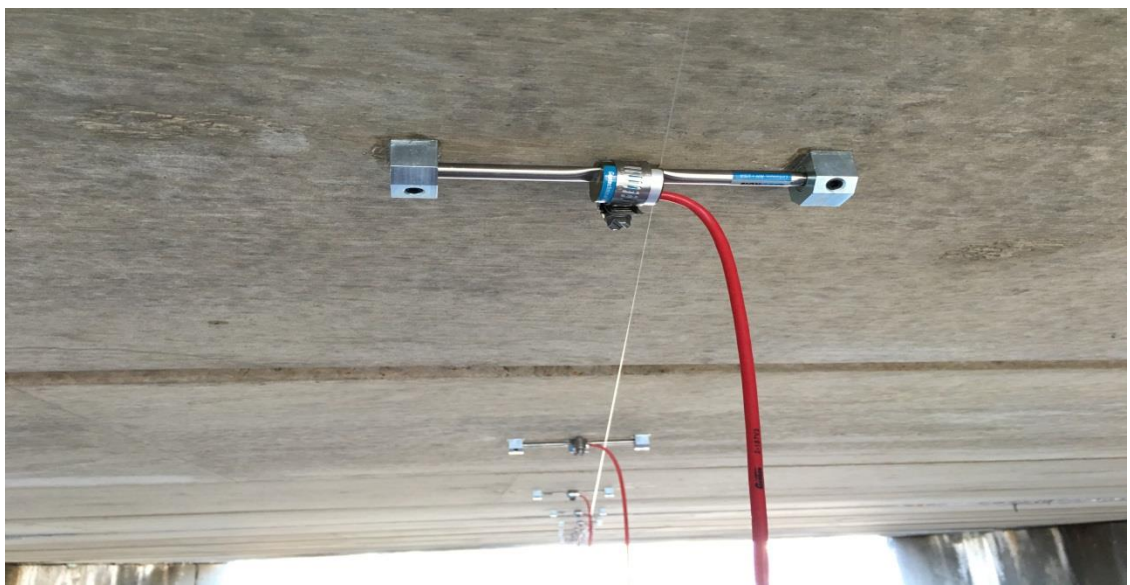


Figure 4.15 - Installed 4000 Vibrating wire strain Gauges

After the sensors were installed, the 2-axle pre-loaded dump truck was used, the truck path decided by the sensors location. Three types of tests (parking test, crawling test, and dynamic test) were performed through four spans of the bridge, and each type of test has been performed three times to confirm data reproducibility and to establish the reliable characteristics of the beams' behavior. The parking test was done by setting the truck in the middle of the span for five minutes, the crawling test was done by driving the truck 5 miles/hour over the span, and the dynamic test was done by drive the truck 30 miles/ hour through the path. When the truck was crossing over the structure, the sensors recorded the data simultaneously to the CR6 data logger, and the data was collected to the laptop by using the LoggerNet software program. The data logger collected data for the strain gages and the PTs every 0.2 seconds (200 milliseconds), its mean recorded five times per second.



Figure 4.16 - Installed 4000 Vibrating wire strain Gauges and PT 8510

Test Vehicle:

The weights and dimensions of the test vehicle were recorded before the investigation. The live load was the weight of the vehicle in the station; the vehicle's total weight was 57,800 lbs. It is a three-axle truck, with a front-wheel weight of 9 kips for each wheel, a rear-wheel weight of 10 kips for each wheel, and a middle-wheel weight of 10 kips for each wheel. The distance between the front and middle wheels is 16'9" and the distance between the middle and a rear wheel is 4'9". Figure 4.17 shows the distances and the weights. The truck driver was instructed to drive along the path designated by paint marks for each trip.



Figure 4.17 - The weights and distances for the load vehicle

4.5 Result of live load test

The data logger program began to collect data from CR6. As the CR6 data logger collected data from sensors, the test vehicle started its journey. The data was recorded onto a laptop computer in raw form. The raw data collected from strain gauges was converted to strain data using a pre-coded program, while the raw data collected from the PTs was converted from electrical signals to displacement values by using a preceded program before being plotted on graphs. The test was carried out for two spans, with each span having 21 beams, while each test had three iterations to ensure data quality. Tables 4.3a and 4.3b below show the maximum strain and maximum displacement for each beam in the middle of the span.

Table 4.3a Data for strain and displacement – Span 1

Beam No.	Park Test 1		Park Test 2		Park Test 3	
	StrainX10 ⁻⁶	Disp.(in)	StrainX10 ⁻⁶	Disp.(in)	StrainX10 ⁻⁶	Disp.(in)
1						
2						
3	16	0.0035	16	0.0035	16	0.0035
4	-	0.0065	-	0.0065	-	0.0065
5	27	0.008	28	0.008	28	0.008
6	27	0.0065	28	0.0065	27	0.0065
7	25		25		25	
8	20		18		19	
9	15		14		15	
10	11		10.5		10.5	
11	8		8.5		8	
12	10		10		11	
13	13		13		15	
14	19		19		21	
15	23		24		25	
16	22	0.003	23	0.003	23	0.003
17	26.5	0.008	27	0.008	28	0.008
18	15.5	0.005	16	0.005	16	0.005
19	17	0.003	17.5	0.003	18	0.003
20						
21						

Beam No.	Crawing Test 1		Crawing Test 2		Crawing Test 3	
	StrainX10 ⁻⁶	Disp.	StrainX10 ⁻⁶	Disp.	StrainX10 ⁻⁶	Disp.
1						
2						
3	16	0.006	17	0.006	18	0.006
4	6.5	0.004	7	0.004	6.5	0.004
5	22	0.004	23	0.004	22	0.004
6	22	0.006	23	0.006	23	0.006
7	18		18		18	
8	16		14		14	
9	15		12		14	
10	12		10		12	
11	12		8		13	
12	13		10		14	
13	16		12		14	
14	17		14		14	
15	20		20		20	
16	24	0.0065	25	0.0065	25	0.0065
17	24	0.0045	25	0.0045	25	0.0045
18	7	0.004	7.5	0.004	7	0.004
19	17	0.0065	18	0.0065	19	0.0065
20						
21						

Beam No.	Dynamic Test 1		Dynamic Test 2		Dynamic Test 3	
	StrainX10 ⁻⁶	Disp.(in)	StrainX10 ⁻⁶	Disp.(in)	StrainX10 ⁻⁶	Disp.(in)
1						
2						
3	14	0.0055	15	0.0055	16	0.0055
4	-	0.005	-	0.005	-	0.005
5	23	0.005	26	0.005	25	0.005
6	25	0.008	27	0.008	23	0.008
7	22		25		20	
8	17		18		15	
9	12		15		10	
10	8		9		7	
11	6		7		7	
12	8		10		8	
13	11		13		15	
14	17		18		17	
15	23		24		24	
16	25	0.003	25	0.003	25	0.003
17	26	0.0075	26	0.0075	27	0.0075
18	18	0.006	17.5	0.006	18.5	0.006
19	19	0.003	18	0.003	21	0.003
20						
21						

Table 4.3b Data for strain and displacement – Span 2

Beam No.	Park Test 1		Park Test 2		Park Test 3	
	StrainX10-6	Disp.	StrainX10-6	Disp.	StrainX10-6	Disp.
1						
2						
3	15	0.005	16	0.005	15	0.005
4	6	0.004	6.5	0.004	5	0.004
5	21	0.004	21	0.004	22	0.004
6	22	0.0045	23	0.0045	23	0.0045
7	17		19		20	
8	13		14		15	
9	11		14		13	
10	8		10		9	
11	7		8		8	
12	8		8		10	
13	12		10		13	
14	16		12		15	
15	18		16		17	
16	20	0.006	21	0.006	25	0.006
17	25	0.004	20	0.004	25	0.004
18	6	0.004	5	0.004	6	0.004
19	18	0.005	15	0.005	19	0.005
20						
21						

Beam No.	Crawling Test 1		Crawling Test 2		Crawling Test 3	
	StrainX10-6	Disp.	StrainX10-6	Disp.	StrainX10-6	Disp.
1						
2						
3	16	0.006	17	0.006	18	0.006
4	6.5	0.004	7	0.004	6.5	0.004
5	22	0.004	23	0.004	22	0.004
6	22	0.006	23	0.006	23	0.006
7	18		18		18	
8	16		14		14	
9	15		12		14	
10	12		10		12	
11	12		8		13	
12	13		10		14	
13	16		12		14	
14	17		14		14	
15	20		20		20	
16	24	0.0065	25	0.0065	25	0.0065
17	24	0.0045	25	0.0045	25	0.0045
18	7	0.004	7.5	0.004	7	0.004
19	17	0.0065	18	0.0065	19	0.0065
20						
21						

Beam No.	Dynamic Test 1		Dynamic Test 2		Dynamic Test 3	
	StrainX10 ⁻⁶	Disp.	StrainX10 ⁻⁶	Disp.	StrainX10 ⁻⁶	Disp.
1						
2						
3	20	0.004	15	0.004	18	0.004
4	6	0.0045	5	0.0045	5.5	0.0045
5	25	0.006	20	0.006	25	0.006
6	25	0.0045	20	0.0045	25	0.0045
7	21		15		21	
8	16		12		16	
9	14		12		12	
10	11		11		10	
11	9		9		9	
12	7		7		8	
13	10		10		10	
14	13		13		13	
15	x		x		x	
16	21	0.009	22	0.009	21	0.009
17	22	0.011	23	0.011	22	0.011
18	x	0.008	x	0.008	x	0.008
19	x	0.009	x	0.009	x	0.009
20						
21						

Beams 3, 4, 5, and 6 were chosen to plot and show the differences in strain between the damaged beams (3 and 4) and the intact beams (5 and 6). Figure (4.15) describes the data that was recorded in the field test. The first max strain (Max 1) location was the point at which the front wheels of the test vehicle crossed the sensor location for the first beam (Beam 6), Also the same value maximum strain for the second beam (Beam 5) was recorded. In the same manner, the second max strain (Max 2) location was the point at which the rear wheels of test vehicle crossed the sensor location for Beams 5 and 6. The third maximum strain (Max 3) location was where the rear wheels of the test vehicle crossed the sensor location for Beam 3. The fourth max strain (Max 4) location was where the rear wheel of the test vehicle crossed the sensor location for Beam 4. All strains are shown in Figure (4.18).

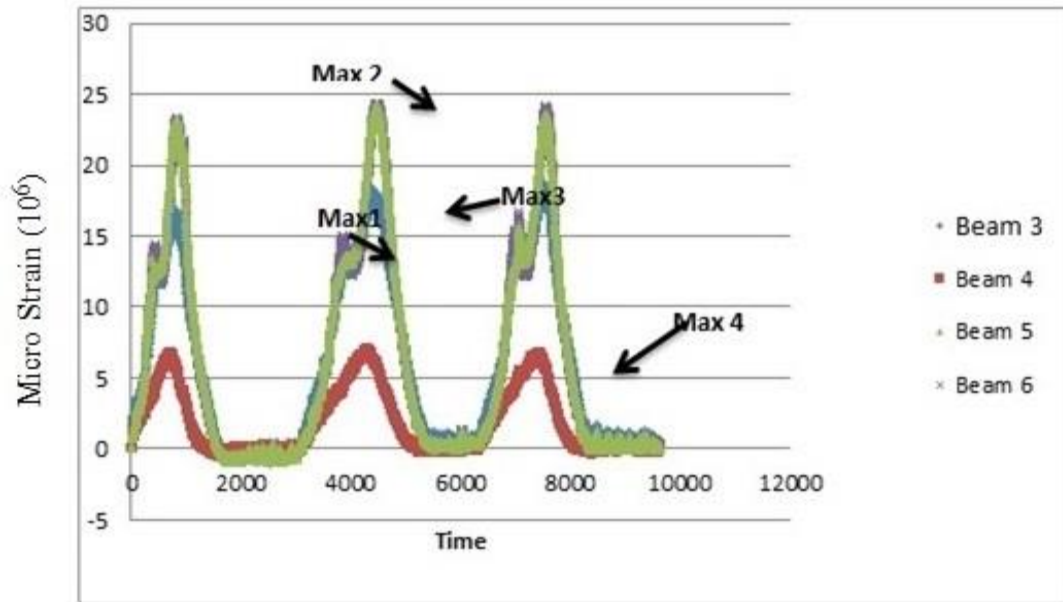


Figure 4.18 - Strain gauges scrawling for Beams 3, 4, 5, and 6

As indicated in Figure 4.18, there is a difference between the intact beams (5 and 6) and the damaged beams (3 and 4). The max strain of both intact beams shows a similar trend of higher strain under the heavier (rear-wheel) load than under the front wheels. Moreover, the strain for the intact beams is higher than the strains shown for the damaged beams.

Chapter Five

Analytical Computations

This chapter provides details of analytical procedure to estimate the strains measured during the load test testing. This study was conducted to find the influence of many variables on the value of the strain. There are many variables have significant effect to change the value of the correct strain. The various steps are:

- Distribution load sharing among the beams and beam properties.
- Computation maximum Absolut moment among the beam.
- Properties of cross section.
- Computation of maximum strain.
- Variables that affect maximum strain.
- Use of these variables for accurate prediction of maximum strain.

These variables are calculated to compare with the strain that has gotten from the load-test in the site. Beam number 7 from the Table 3.3a was used for the parametric study. The maximum strain for this beam was 25 micro.

5.1 Load (sharing) distribution among beams and beam properties

The wheel load is distributing unequally between the adjacent girders. In this part, the maximum load distribution factor has been calculated by the area under the strain-distance curve in Figure 5.1 as follow:

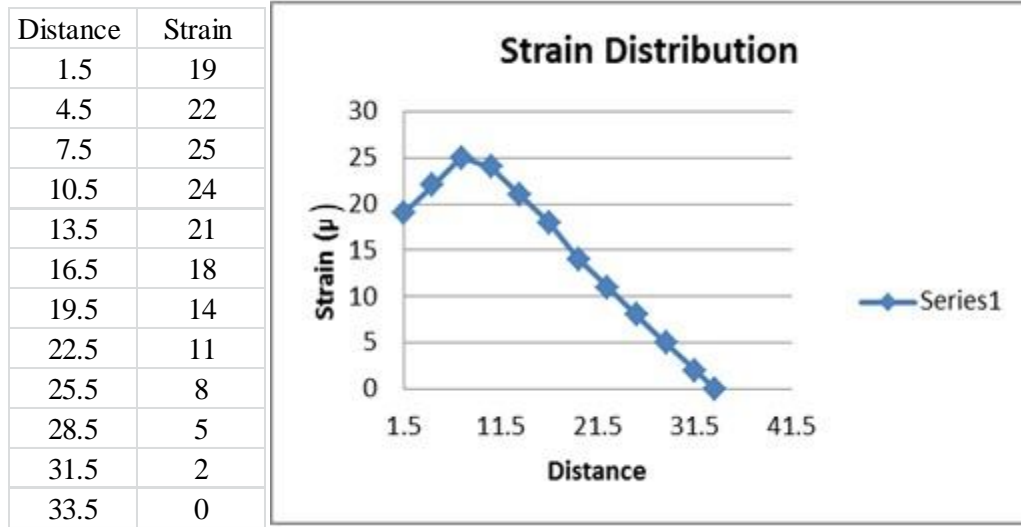


Figure 5.1 - Strains along the cross section of the bridge

Total area under curve = 173

Maximum strain = 25

$$\text{Distribution factor \%} = \frac{25}{173} * 100\% = 14.5\%$$

Check I_g :

$$I_g = 112 [36 * 27^3 - 26.75 * 16^3] = 49,918.3 \text{ in}^4$$

$$y = \frac{14 * A * 0 + 10 * A * 8.175 + 2 * A * 3.5}{26 A} = 0.94 \text{ in}$$

$$\bar{y} = \frac{4 * A * 0 + 2 * A * 3.5}{6 * A} = 1.17''$$

$$n = E_s E_c = \frac{29,000 * 10^3}{57,000 \sqrt{5000}} = 7.2$$

$$A_{c_{tr}} = A_s * n$$

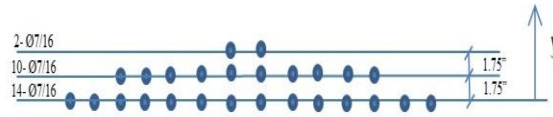


Figure 5.2 - Bottom bars

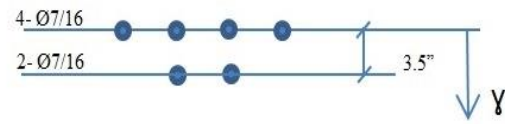


Figure 5.3 - Top bars

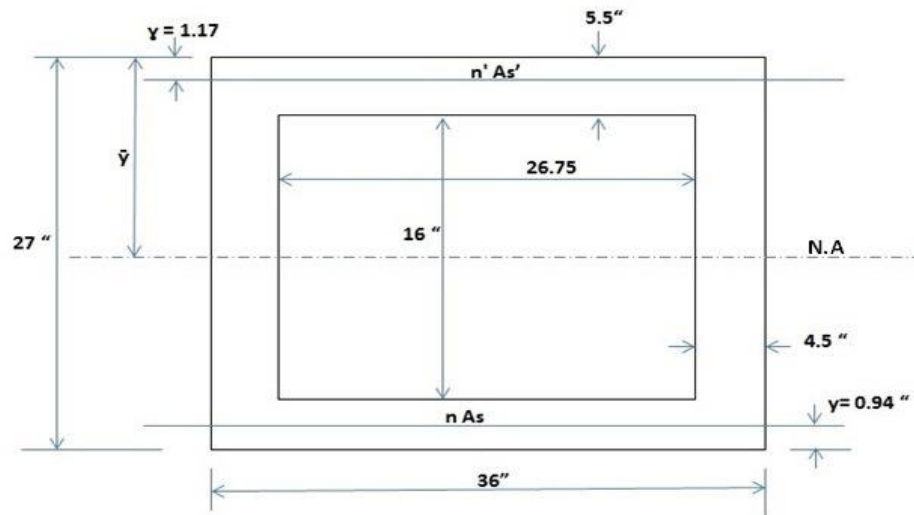


Figure 5.4 - cross section in box-girder

$$\bar{y} = (n' * As' * y + n * As * (27 - 0.94) + (4.5 * 27 * \frac{27}{2}) * 2 + 26.75 * 5.5 * 5.5/2 + 26.75 * 5.5 * (27 - \frac{5.5}{2}) / (\Sigma A = 544 + n - 1As + n - 2As')$$

$$\bar{y} = 14''$$

$$I_{tr} = nAs * (27 - 2.94 - \bar{y})^2 + n'As' * (\bar{y} - y)^2 + (36 * 27^3 / 12) + 36 * 27 * (27/2 - \bar{y})^2 - 26.75 * 16^3 / 12 - 26.75 * 16 * (27/2 - \bar{y})^2$$

$$I_{tr} = 53,051 \text{ in}^4$$

$$f_t = \frac{470.4 * 12}{49918} * \frac{27}{2} = 1.53 \text{ K/in}^2 = 1530 \text{ lb/in}^2$$

$$E_c = 57000 * 5000 = 4030.5 \text{ Ksi}$$

$$\epsilon = \frac{1.53}{4030.5} = 0.38 * 10^{-3} = 380 \text{ micro strain}$$

Reduced strain after applying the distribution factor was:

$$0.145 * 380 = 55.1$$

The obtained strain from analysis 55.1μm was higher than the reported strain from the field test 25 μm. There were many reasons for that. First, the end restriction of the span may cause reduction in the strain. In the analysis, the bridge assumed simply supported without any restriction at the ends, however, in the real case there were some restrictions due to the continuity of the bridge deck. Furthermore, the expected modulus of elasticity was higher than the calculated one because the section was prestressed, so the concrete may be compressed and increase the modulus of elasticity. Moreover, the real inertia of the section was higher than the calculated inertia because of the extra mild steel, also prestressed strands. Finally, the effect of compression stress due to prestressed strands in the tension zone had not been considered in the analysis, and this might be the major reason for the difference.

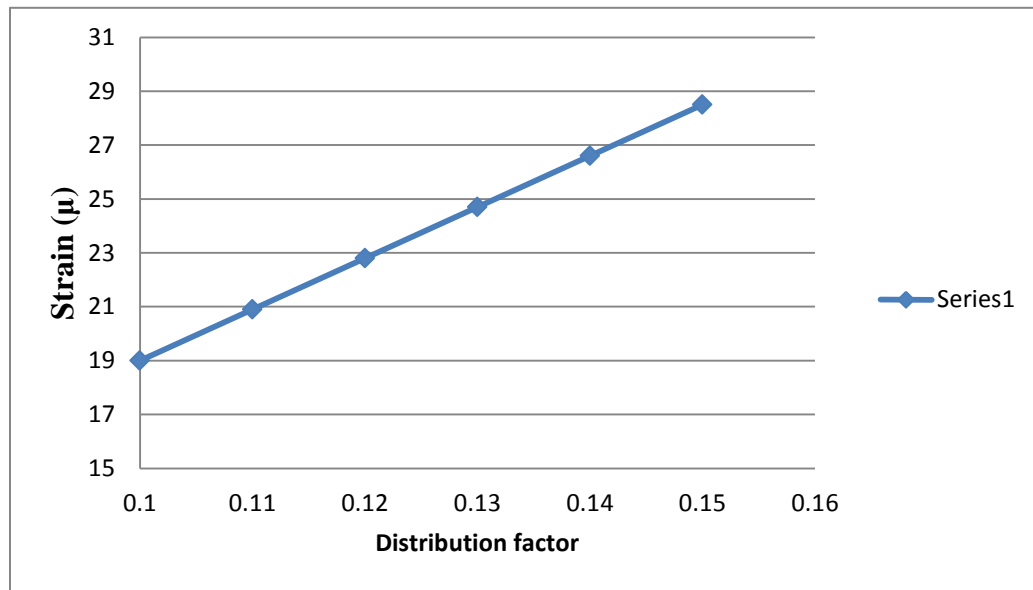


Figure 5.5 - The relation between the distribution factor and strain

5.2. A. Maximum Absolut Moment

The theoretical maximum absolute moment have been calculated using the same wheel load from the truck was used in the field test. The wheel load shown in the Figure 5.2.

Input:

$$P_1 = 20K$$

$$P_2 = 20K$$

$$P_3 = 18K$$

$$L = 46ft$$

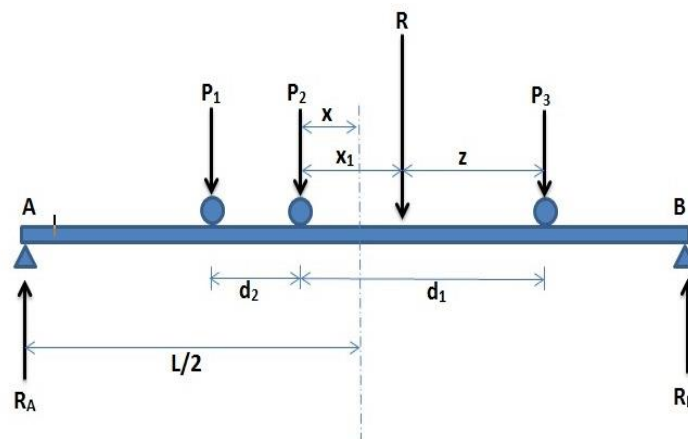


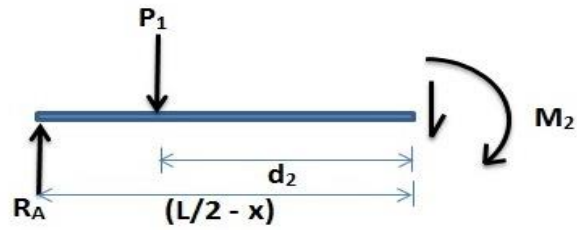
Figure 5.6 - vehicle test location on the bridge

$$D1=16'-9''$$

$$D2=4'-9''$$

$$R=P1+P2+P3=58K$$

$$\Sigma M_B = 0 \quad + \curvearrowright$$



$$R_A = 1LR \quad L2 - X1 - X \dots\dots\dots (1)$$

$$M_2 = R_A \left[\frac{L}{2} - X \right] - P_1 d_2 \dots\dots\dots (2)$$

Sub (1) Into (2):

$$M_2 = RL \quad L22 - X1L2 + XL2 - XL2 + X1X1 - x2 - P_1 d_2$$

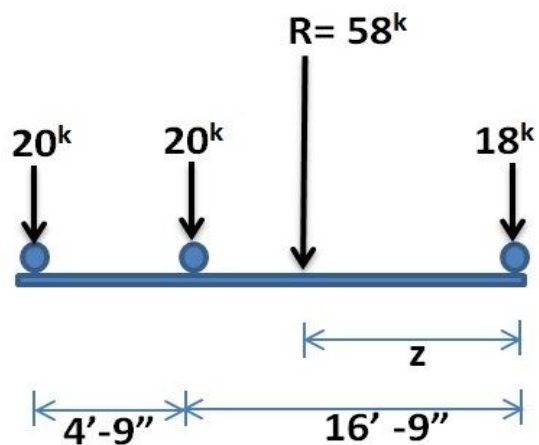
$$\frac{dM_2}{dx} = 0 \quad (\text{For Max. } M_2)$$

$$dM_2/dx = RL \quad 0 - 0 - X1 - 2X - 0 = 0$$

$$x = \frac{X1}{2}$$

Also,

$$z = \frac{20 \times 21.5 + 20 \times 16.75}{58} = 13.1 \text{ ft}$$



$$x_1 = 16.75 - 13.1 = 3.65'$$

$$x = x1/2 = 3.65/2 = 1.825'$$

$$L = 46 \text{ ft} , R = 58^k$$

$$R_A = \frac{58}{46} \left[\frac{46}{2} - (3.65 - 1.825) \right]$$

$$R_A = 26.7^k \quad (\text{maximum expected reaction on the left pier})$$

$$M_L = 26.7 * 21.175 - 20 * 4.75$$

$$M_L = 470.4 \text{ K.ft}$$

This moment represents the maximum moment if the beam resists the entire load. Since the load is shared by other beams, the moment resisted by the damaged beam is estimated using the procedure presents in the next section.

$$M_L = 0.145 * 470.4 = 68.2 \text{ K.ft}$$

5.2. B. Another Approach to find M:

In this approach, the maximum moment has been calculated assuming the load is symmetric and the maximum moment in the middle of the span.

$$M = 20 * 20.635 = 412.7 \text{ K.ft}$$

$$F'_c = 5000 \text{ psi}$$

$$I_g = 49,918 \text{ in}^4, A = 544 \text{ in}^2 A_{(\text{strand } \varnothing 7/16)} = 0.115 \text{ in}^2$$

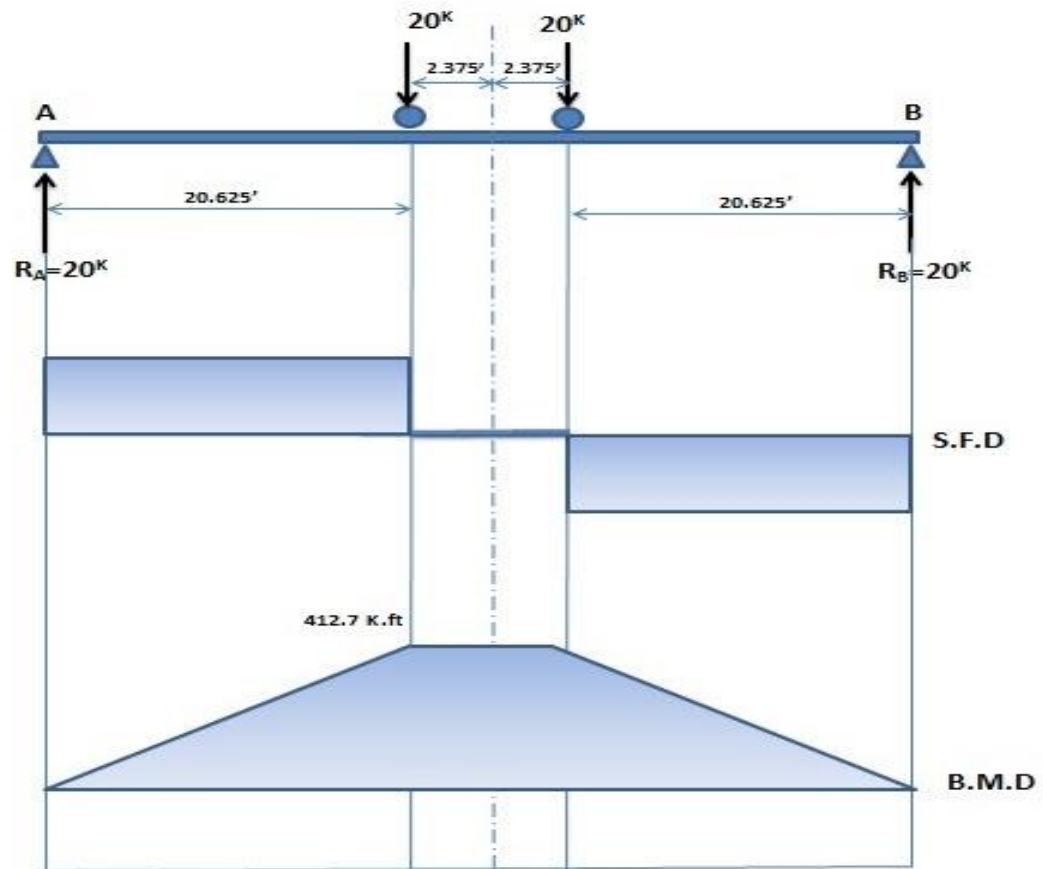


Figure 5.7 - SFD and BMD for the beam

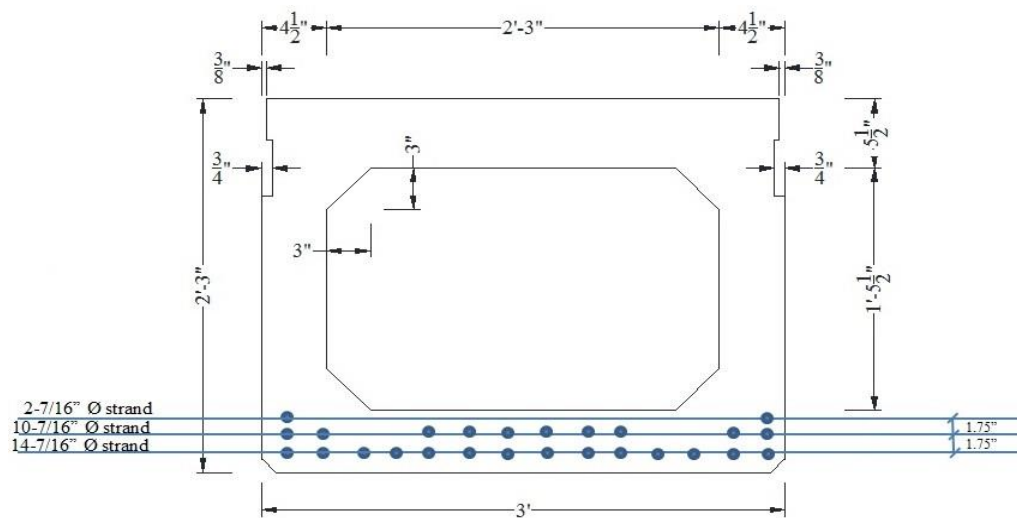


Figure 5.8 - cross section in box-girder with bottom reinforcement

5.3.1 Influence of Asphalt layer on Distribution of load among the girder

In this part, the influence of the thickness of the asphalt layer on the concrete deck has been included:

$$I_g = 49,918 \text{ in}^4$$

$$n = n' = E_s/E_c = \frac{29,000 * 10^3}{57000 \sqrt{5000}} = 7.2$$

$$A_{c_{tr}} = A_s * n_{asph.}$$

$$n_1 = E_{asph.}/E_c = \frac{1 * 10^6}{57000 \sqrt{5000}} = 0.25$$

$$\bar{y} = \frac{n' * A_s' * (y + 6) + n * A_s * (33 - 0.94) + \left(4.5 * 27 * \left(\frac{27}{2} + 6 \right) \right) * 2 + 26.75 * 5.5 * \left(\frac{5.5}{2} + 6 \right) + 26.75 * 5.5 * \left(33 - \frac{5.5}{2} \right) + 6 * 9 * 3}{\Sigma A = 544 + (n - 1)A_s + (n - 2)A_s' + n_1 A_{asph.}}$$

$$\bar{y} = 18.5 \text{ “}$$

$$I_{tr} = n * A_s * (33 - 2.94 - \bar{y})^2 + n' * A_s' * (\bar{y} - (1.17 + 6))^2 + 36 * 27^3 / 12 + 36 * 27 * (12.5 - 27/2)^2 - 26.75 * 16^3 / 12 - 26.75 * 16 * (16/2 - 7)^2 + 6 * 9^3 / 12 + 6 * 9 * (18.5 - 6/2)^2$$

$$I_{tr} = 67,728 \text{ in}^4$$

$$f_t = \frac{235.18 * 12}{67,728} * (33 - 18.5) = 0.6 \text{ k/in}^2$$

$$\epsilon = \frac{0.6}{4030.5} = 0.15 * 10^{-3} = 150 \text{ micro strain}$$

Also,

E (Asphalt) psi	Strain (Micro strain)
$0.5 * 10^6$	160
$0.75 * 10^6$	155
$1 * 10^6$	150
$1.25 * 10^6$	144
$1.5 * 10^6$	138

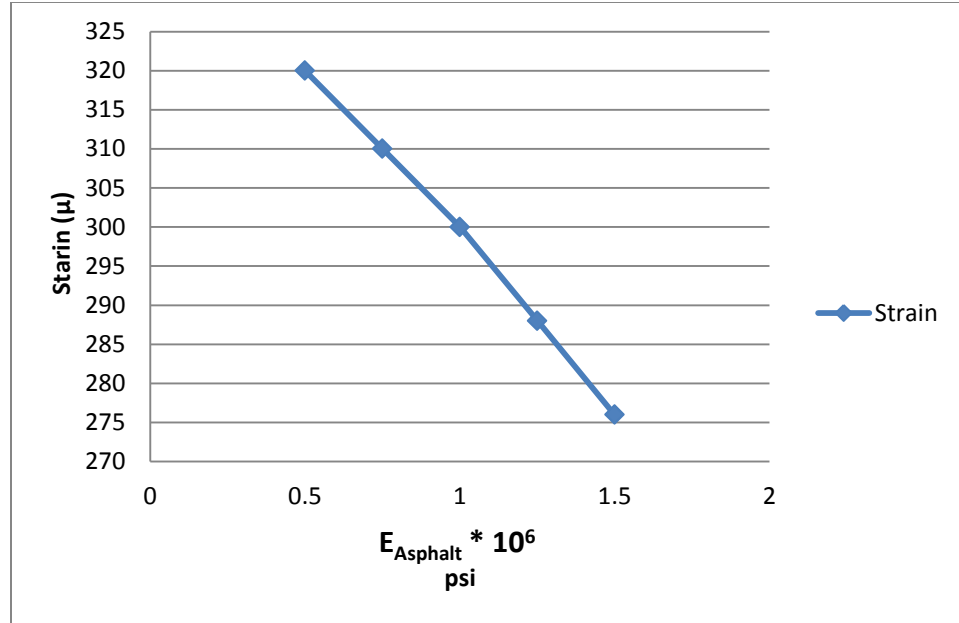


Figure 5.9 - The relation between the Asphalt's Modulus of elasticity and strain

5.3.2 Prestress force from the bottom strand

To include the effect of prestress force on the strain of the girder from the bottom strand, eight strand were assumed deteriorated.

Then,

The total workable strands in the girder = $26 - 8 = 18$ strands

$$P = 18 * 0.115 * 120 = 248.4 \text{ K}$$

$$e = 33 - 18.5 - 0.94 = 13.56 \text{ in}$$

$$M_e = 248.4 * 13.56 / 12 = 281 \text{ K/in}^2$$

$$\begin{aligned} f_{\text{bottom}} &= \frac{P}{A_g} - \frac{e}{I_g} * (M_e - M_L) \\ &= \frac{248.4}{544} - \frac{33-18.5}{67728} * (281 - 235.18) = 0.447 \text{ K/in}^2 \end{aligned}$$

$$\epsilon = \frac{0.447}{4030.5} = 0.11 * 10^{-3} = 110 \text{ micro strain}$$

5.3.3 Fixed end moment

In the ideal case the maximum moment was calculated assuming there wasn't any restriction at the ends. In the real case there was a significant effect for this restriction. To include the effect of end restrain for possible zero moment were discussed, and the results shown in Figure 5.10.

$$1- 0.975L = 44.85 \text{ ft}$$

$$R_A = \frac{29}{44.85} * \left(\frac{44.85}{2} - (3.65 - 1.825) \right) = 13.32 \text{ K}$$

$$M = 13.32 * 20.6 - 10 * 4.75 = 227 \text{ k.ft}$$

$$f_t = \frac{227 * 12}{49918} * \frac{27}{2} = 0.74 \text{ k/in}^2$$

$$\epsilon = \frac{0.74}{4030.5} = 0.183 * 10^{-3} = 183 \text{ micro strain}$$

$$2- 0.95L = 43.7 \text{ ft}$$

$$R_A = \frac{29}{43.7} * \left(\frac{43.7}{2} - (3.65 - 1.825) \right) = 13.29 \text{ K}$$

$$M = 13.29 * 20.025 - 10 * 4.75 = 218.6 \text{ k.ft}$$

$$f_t = \frac{218.6 * 12}{49918} * \frac{27}{2} = 0.71 \text{ k/in}^2$$

$$\epsilon = \frac{0.71}{4030.5} = 0.176 * 10^{-3} = 176 \text{ micro strain}$$

$$3- 0.925L = 42.55 \text{ ft}$$

$$R_A = \frac{29}{42.55} * \left(\frac{42.55}{2} - (3.65 - 1.825) \right) = 13.26 \text{ K}$$

$$M = 13.26 * 19.45 - 10 * 4.75 = 210.4 \text{ k.ft}$$

$$f_t = \frac{210.4 * 12}{49918} * \frac{27}{2} = 0.68 \text{ k/in}^2$$

$$\epsilon = \frac{0.68}{4030.5} = 0.169 * 10^{-3} = 169 \text{ micro strain}$$

$$4- 0.9L = 41.4 \text{ ft}$$

$$R_A = \frac{29}{41.4} * \left(\frac{41.4}{2} - (3.65 - 1.825) \right) = 13.22 \text{ K}$$

$$M = 13.22 * 18.875 - 10 * 4.75 = 202 \text{ k.ft}$$

$$f_t = \frac{202 * 12}{49918} * \frac{27}{2} = 0.65 \text{ k/in}^2$$

$$\epsilon = \frac{0.65}{4030.5} = 0.162 * 10^{-3} = 162 \text{ micro strain}$$

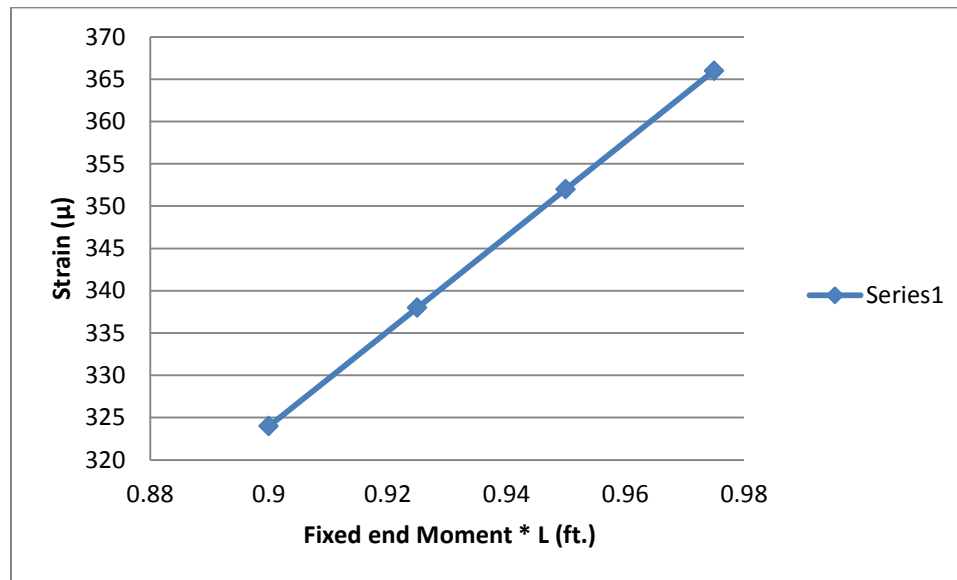


Figure 5.10 - The relationship between the fixed end moment and the strain

Chapter Six

Study for alternative solution for the bridge

6.1 Introduction:

In the box- girder adjacent bridge that we have investigated in this study, the water ingress to the joint between girders and caused a sever deterioration to the box-girders of the bridge. The type of the geometry and the shear key that connected the box-girders of the bridge to each other may the main reason for this deterioration by holding the water in place.

In the original geometry, the bridge was consisting of four spans with total span length equal to 236 ft. the second and the fourth pier were deteriorated severely. For that, an alternative geometry for the spans has been proposed. The proposed new span geometry has two equal spans with 120 ft. each and one pier in the middle.

Moreover, an alternative geometry for the girders has been suggested in this study in case of any future plan to replace the bridge. Type IV precast prestressed concrete beam suggested instated of the box-girder. All the detailed calculations for analysis the new bridge have been elaborated and reported in this chapter.

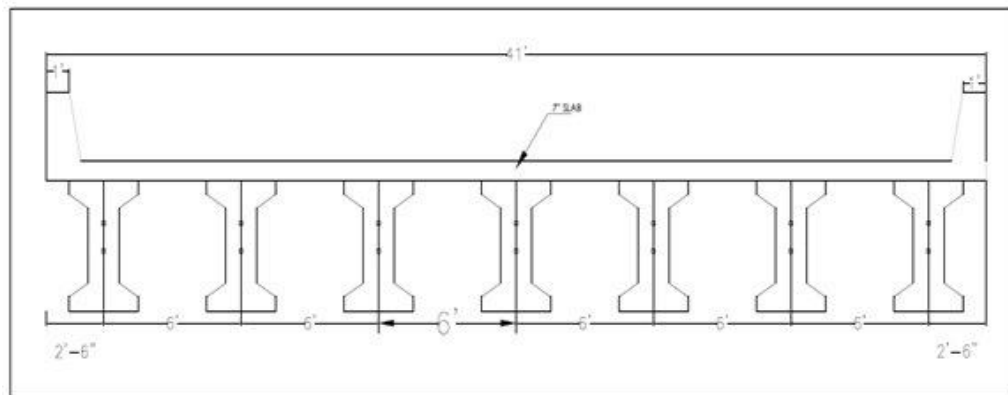


Figure 6.1 - Cross section in bridge deck

Given:-

1. span data:

Overall beam length= 121 ft

Design beam length= 120 ft

- 2- Cross section data:

Number of lanes=2

Number of beams= 7

Beam spacing=6 ft

- 3- Dead loads:

Slab thickness = 7 in

Barrier weight= 0.2 k/ft

Future wearing surface= 0.02 k/ft²

Wearing width=25 ft

Wc=145 lb/ft³

4- Live loads:

HL-93 Design truck +Design lane load

5- Deck properties:

Deck concrete 28- day strength =4 ksi

f'c=4 ksi

$$E_c = 33000w^{1.5}\sqrt{f'_c} = 33000*(0.145)^{1.5}\sqrt{4} = 4074ksi$$

6- Beam properties:

Beam concrete 28- day strength =7 ksi

$$E_c = 33000w^{1.5}\sqrt{f'_c} = 33000*(0.145)^{1.5}\sqrt{7} = 4821ksi$$

Beam concrete strength at release = 6 ksi

$$E_c = 33000w^{1.5}\sqrt{f'_c} = 33000*(0.145)^{1.5}\sqrt{6} = 4463ksi$$

7- Prestressed strand:

0.6 in diameter, 270 ksi low relaxation strand

$A_{ps} = 0.217 \text{ in}^2$ for one strand

$E_{ps} = 28500 \text{ ksi}$

$f_{pu} = 270 \text{ ksi}$

$f_{py} = 0.9 f_{pu} = 0.9 * 270 = 243 \text{ ksi}$

Select standard section:

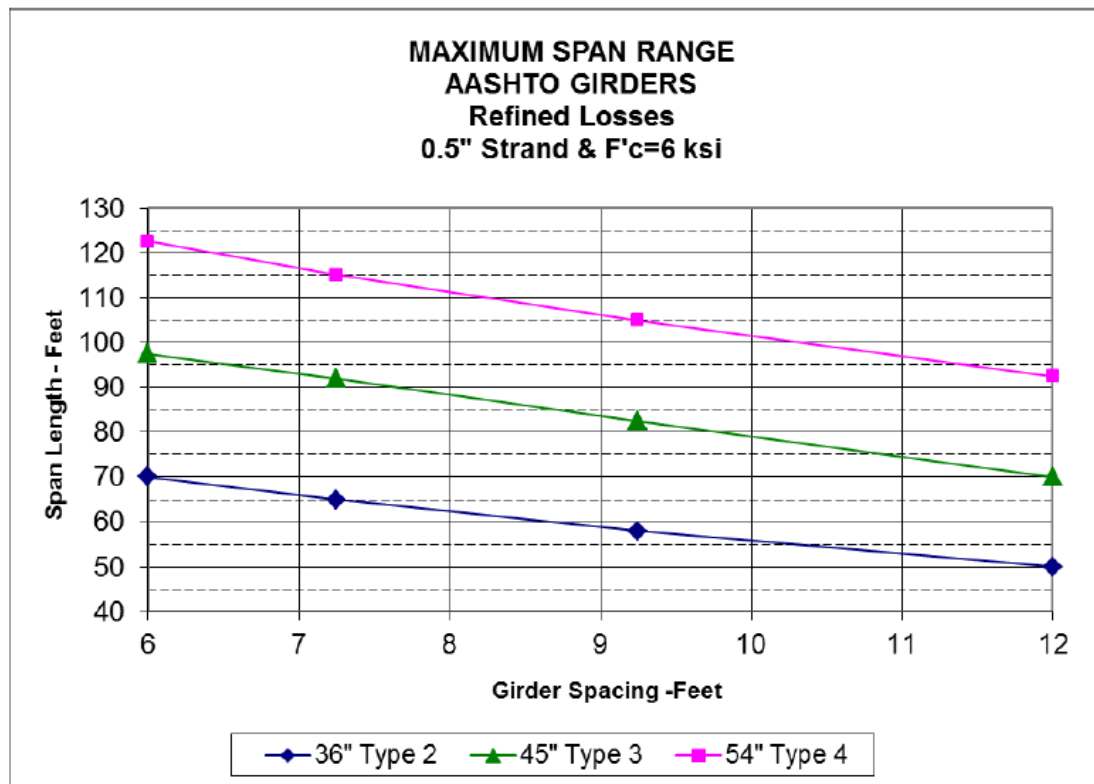


Figure 6.2 - Girder spacing versus span length

From the curve above: with $L = 120 \text{ ft}$ and $S = 6 \text{ ft}$

The best section is (Type 4) with 54 in depth

The properties of sections as elaborated in Table 5.1:

Table 5.1 AASHTO girder section properties

AASHTO GIRDER SECTION PROPERTIES							
DEPTH	AREA	CENTER OF GRAVITY		MOMENT OF INERTIA	SECTION MODULUS		WEIGHT
		TOP	BOTTOM		TOP	BOTTOM	LB/FT
36"	368.44	20.147	15.853	50,842	2524	3207	384
45"	558.94	24.706	20.294	125,165	5066	6168	582
54"	788.44	29.249	24.751	260,403	8903	10,521	821

ALL UNITS IN INCHES EXCEPT WEIGHT

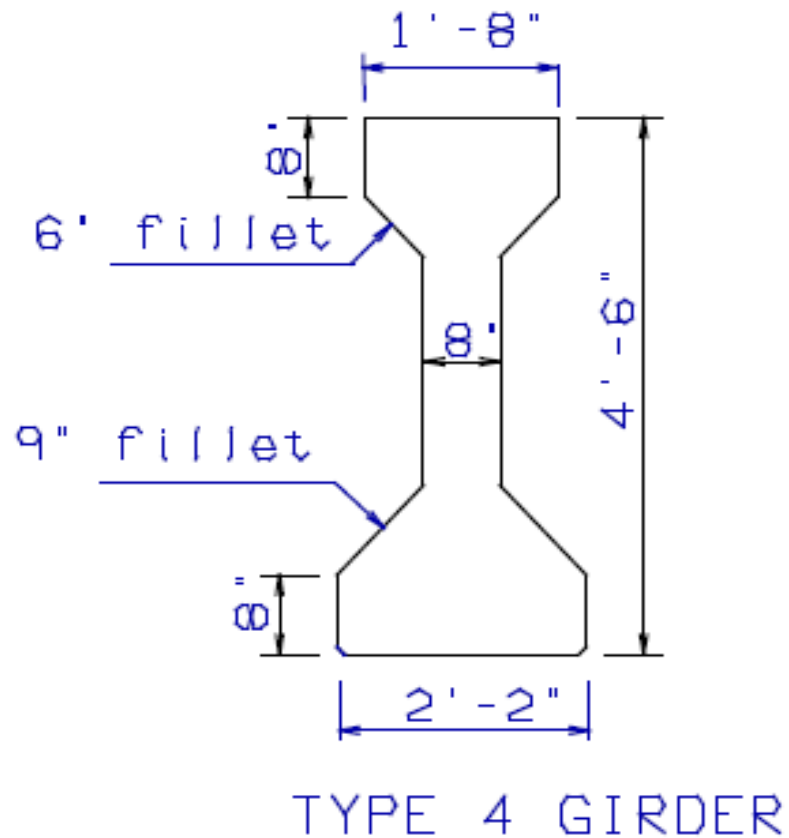


Figure 6.3 - Type 4 girder

Effective flange width – AASHTO (4.6.2.6.1)

A- Interior beam:

For the interior beam, the effective flange width may be taken as the *least* of:

1- One quarter of the effective span length : 120 feet for simple spans

$$(0.25) (120) (12) = 360 \text{ in}$$

2- Twelve time the average thickness of the slab, 7 in , plus the greater of

The web thickness: 8 in

One-half of the top flange of the girder: 42 in

$$(0.5) (20) = 10 \text{ in}$$

The greater of these two values is 10 in and:

$$(12) (7) + (10) = 94 \text{ in}$$

3- The average spacing of adjacent beams: 6 ft

$$(6) (12) = 72 \text{ in}$$

The least of these is 72 in and therefore, *the effective flange width is (72 in).*

B- For the exterior beam, the effective flange width may be taken as one- half the effective flange width of the adjacent beam, 72 in, plus the least of:

1- One-eighth of the effective span length: 120 feet

$$(0.125) (120) (12) = 180 \text{ in}$$

2- Six times the average thickness of the slab: 7 in, plus the greater of:

One-half of the web thickness: 8 in

$$(0.5) (8) = 4 \text{ in}$$

One- quarter of the top flange of the girder: 20 in

$$(0.25) (20) = 5 \text{ in}$$

The greater of these two values is 5 in and:

$$(6) (7) + 5 = 47 \text{ in}$$

3- The width of the overhang: 2.5 ft

$$(2.5) (12) = 30 \text{ in}$$

The least of these is 30 in and *the effective flange width is:*

$$(0.5) (72) + 30 = 66 \text{ in}$$

Composite section properties:

$$n = \frac{E_{deck}}{E_{beam}} = \frac{4074}{4821} = 0.845$$

The transformed deck area is:

$$A = (72) (.845) (7) = 425.88 \text{ in}^2$$

$$I_o = (72) (0.845 (7)^3 / 12 = 1739 \text{ in}^4$$

	A	Yb	Ayb	D	Ad ²	I _o	I _o +Ad ²
Deck	425.9	57.5	24489.25	21.26	192501.52	1739	194240
Beam	788.4	24.75	19512.9	11.49	104084.64	260403	364487
Total	1214.4		44002.15				558727

Property	Interior beam	Exterior beam
I _{comp} (in ⁴)	558727	
y _{bc} (in)	36.24	
y _{tc} (in)	17.76	
y _{slab top} (in)	24.76	
S _{bc} (in ³)	15417.4	
S _{tc} (in ³)	31460	
S _{slab top} (in ³)	22565.7	

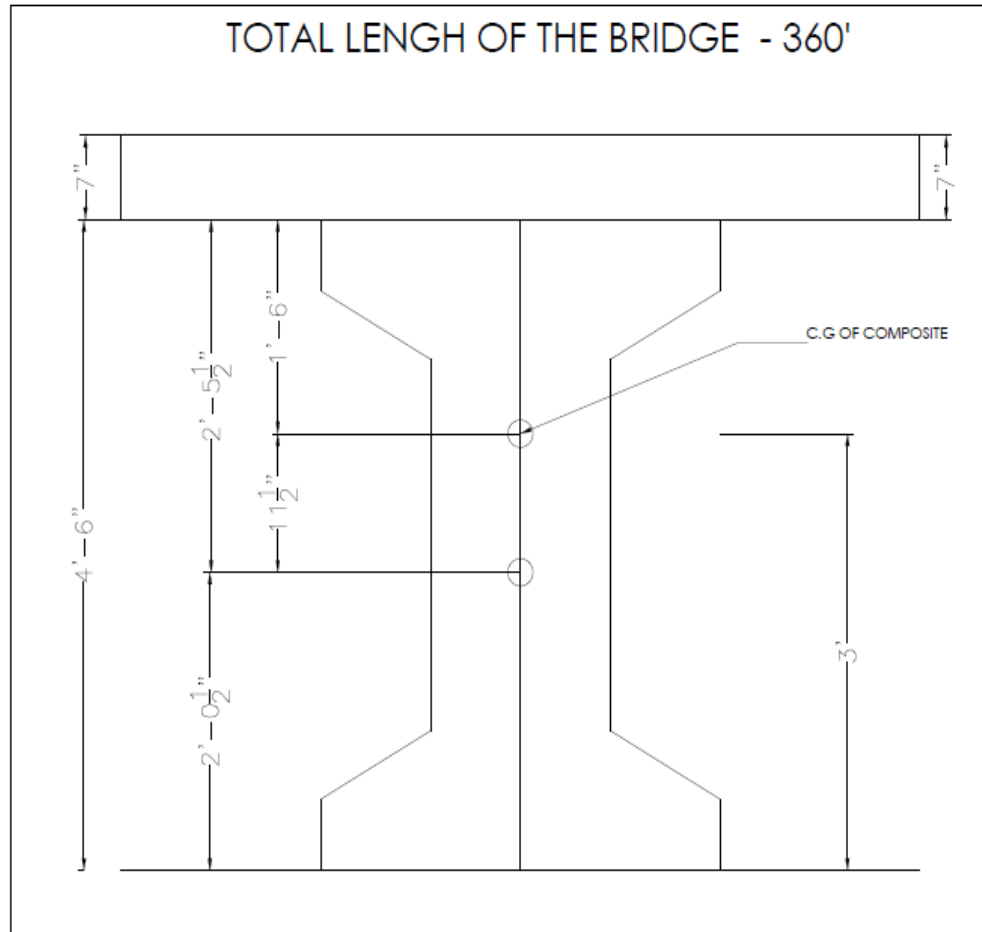


Figure 6.4 - Girder details

Dead loads:

Interior beam

The dead loads, DC, acting on the non-composite section are:

Weight of beam = 0.821 k/ft

Slab weight = $(72/12) (7/12) (0.15) = 0.525$ k/ft

The dead load, DC, acting on the composite section is:

Barrier

$(0.2) (2)/7 = 0.057$ k/ft

The dead load, DC, acting on the composite section is:

Future wearing surface allowance (FWS):

$(0.02) (25)/7 = 0.0714$ k/ft

Distribution of live load:

Interior beam

$eg = yt + ts = 29.249 + 7/2 = 32.75$ in

$$n = \frac{E_{beam}}{E_{deck}} = \frac{4821}{4074} = 1.183$$

The longitudinal stiffness parameter is :

$$K_g = n(I + Ae_g^2) = 1.183(260403 + 788.44 * 32.75^2) = 1308462 in^4$$

Distribution of live load for moment AASHTO (4.6.2.2.2b)

Check the range of applicability

$$3.5 \leq S \leq \quad S = 6ft \quad o.k$$

$$4.5 \leq t_s \leq 12 \quad t_s = 7in \quad o.k$$

$$20 \leq L \leq 240 \quad L = 120ft \quad o.k$$

$$3.5 \leq S \leq \quad S = 6ft \quad o.k$$

$$10000 \leq k_g \leq 7000000 \quad k_g = 1308462in^4 \quad o.k$$

$$N_b \geq 4 \quad N_b = 7 \quad o.k$$

For one lane loaded:

$$g = 0.06 + \left(\frac{S}{14}\right)^{0.4} \left(\frac{S}{L}\right)^{0.3} \left(\frac{K_g}{12Lt_s^3}\right)^{0.1}$$

$$g = 0.06 + \left(\frac{6}{14}\right)^{0.4} \left(\frac{6}{120}\right)^{0.3} \left(\frac{1308462}{12(120)(7)^3}\right)^{0.1} = 0.38$$

For the fatigue limit state, remove the multiple presence factor.

$$g = \frac{0.38}{1.2} = 0.316$$

For two or more design lane loaded:

$$g = 0.075 + \left(\frac{S}{9.5}\right)^{0.6} \left(\frac{S}{L}\right)^{0.2} \left(\frac{K_g}{12Lt_s^3}\right)^{0.1}$$

$$g = 0.075 + \left(\frac{6}{9.5}\right)^{0.6} \left(\frac{6}{120}\right)^{0.2} \left(\frac{1308462}{12(120)(7)^3}\right)^{0.1} = 0.534$$

Distribution of live load for shear:

Check the range of applicability

$$3.5 \leq S \leq \quad S = 6ft \quad o.k$$

$$4.5 \leq t_s \leq 12 \quad t_s = 7in \quad o.k$$

$$20 \leq L \leq 240 \quad L = 120ft \quad o.k$$

$$3.5 \leq S \leq \quad S = 6ft \quad o.k$$

$$10000 \leq k_g \leq 70000000 \quad k_g = 1308462in^4 \quad o.k$$

$$N_b \geq 4 \quad N_b = 7 \quad o.k$$

For one design lane loaded:

$$g = 0.36 + \frac{S}{25} = 0.36 + \frac{6}{25} = 0.6$$

For the fatigue limit state, remove the multiple presence factor.

$$g = \frac{0.6}{1.2} = 0.5$$

For two or more design lane loaded:

$$g = 0.2 + \frac{S}{12} - \left(\frac{S}{35} \right)^2 = 0.2 + \frac{6}{25} - \left(\frac{6}{35} \right)^2 = 0.67$$

Limit states:

The most common limit states for prestressed concrete beam design are:

Strength I

$$1.25\text{DC} + 1.5\text{DW} + 1.75(\text{LL} + \text{IM})$$

Strength II

$$1.25\text{DC} + 1.5\text{DW} + 1.35(\text{LL} + \text{IM})$$

Service I

$$1.0\text{DC} + 1.0\text{DW} + 1.0(\text{LL} + \text{IM})$$

Service III

$$1.0\text{DC} + 1.0\text{DW} + 0.8(\text{LL} + \text{IM})$$

Fatigue

$$0.75(\text{LL} + \text{IM})$$

Beam stresses:

In order to determine the number of required strands, first calculate the maximum tensile stress in the beam for Service III limit state. The number of required strands is usually controlled by the maximum tensile stresses in the beam meet the tensile stress limit. For simple span beams, the maximum tensile force is at mid span at the extreme bottom beam fiber. The tension service stress at the bottom beam fibers can be calculated using:

$$f_{bottom} = -\frac{M_{beam} + M_{slab}}{S_b} - \frac{M_{barrier} + M_{FWS} + 0.8M_{LL}}{S_{bc}}$$

(Service III limit state)

The non-composite moments are:

$$M_{beam} = \frac{0.821 * 120^2}{8} = 1478k.ft$$

$$M_{slab} = \frac{0.525 * 120^2}{8} = 945k.ft$$

The composite moments are:

$$M_{barrier} = \frac{0.057 * 120^2}{8} = 102.6k.ft$$

$$M_{FWS} = \frac{0.0714 * 120^2}{8} = 128.5k.ft$$

Live load plus dynamic load allowance :(HL-93)

$$M_{LL+I} = DF(M_{lane} + 1.33M_{truck})$$

$$M_{lane} = \frac{0.64 * 120^2}{8} = 1152k.ft$$

$$M_{truck} = 1883k.ft$$

$$M_{LL+I} = 0.534(1152 + 1.33 * 1883) = 1952k.ft$$

Interior beam- stresses due to dead load and live load.

$$f_{bottom} = \left(-\frac{1478 + 945}{10521} - \frac{102.6 + 128.5 + 0.8 * 1952}{15417.4} \right) * 12 = -4.16ksi(t)$$

Preliminary strand arrangement:

The development of a strand pattern is a cyclic process. Two design parameter need to be initially estimated: the total prestress losses and the eccentricity of the strand pattern at mid span.

The total required prestress force can be calculated using:

$$P_e = \frac{f_{ten} - f_{bottom}}{\left(\frac{1}{A} - \frac{e}{S_{bmc}} \right)}$$

The concrete stress limit for tension, all loads applied, and subjected to severe corrosion condition table (5.9.4.2.2-1), is

$$f_{ten} = 0.0948\sqrt{f'_c} = 0.0948\sqrt{7} = 0.25ksi$$

$$\Delta f_{pT} = 35ksi \quad (estimated)$$

$$f_{pj} = (0.75)(270) = 202.5ksi$$

$$f_{pe} = 202.5 - 35 = 167.5ksi$$

$$P_e = f_{pe} * A_{ps} = 167.5 * 0.217 = 36.34k \quad (\text{For one strand})$$

$$P_e = \frac{-0.25 - (-4.16)}{\left(\frac{1}{788.4} - \frac{(-20)}{10521} \right)} = 1233.7k$$

e = -20 inches (estimated)

The number of strand required is:

$$\frac{1233.7}{36.34} = 33.94$$

Try use 34 strands.

The distance from the bottom of the beam to the center of gravity of the prestressing strands is:

$$y^- = \frac{10 * 2 + 10 * 4 + 10 * 6 + 4 * 8}{34} = 4.75in$$

The eccentricity of the prestressing strands at the midspan is:

$$e = 24.75 - 4.75 = 20 \text{ in}$$

At the ends of the beam the distance from the bottom of the beam to the center of gravity of the prestressing strands with 10 strand harped at the 0.4 span point, is:

$$y^- = \frac{8 * 2 + 8 * 4 + 8 * 6 + 2(52 + 50 + 48 + 46 + 44)}{34} = 16.94in$$

The eccentricity of the prestressing strands at ends of the beam is:

$$e = 24.75 - 16.94 = 7.81 \text{ in}$$

Prestress loss- Low relaxation strand

We will assume that the prestressing strands are jacked to an initial stress of 0.75fpu

Girder creep coefficients for final time due to loading at transfer

$$H=70\%$$

$$V/S= 4.5$$

$$t_i= 1 \text{ day}$$

$$t_f=20000 \text{ days}$$

$$t=20000-1=19999 \text{ days}$$

$$K_{vs} = 1.45 - 0.13(V / S) = 1.45 - 0.13(4.5) = 0.865$$

$$K_{hc} = 1.56 - 0.008H = 1.56 - 0.008 * 70 = 1$$

$$K_f = \frac{5}{1 + f'_c} = \frac{5}{1 + 6} = 0.7142 \quad K_{td} = \left(\frac{t}{61 - 4f'_c + t} \right) = \frac{19999}{61 - 4(6) + 19999} = 0.9981$$

$$\psi(t_f, t_i) = 1.9 K_{vs} K_{hc} K_f K_{td} t_i^{-0.118}$$

$$\psi(t_f, t_i) = 1.9(0.865)(1)(0.7142)(0.9981)(1)^{-0.118} = 1.1715$$

Girder creep coefficient at time of deck placement due to loading introduced at transfer

$$t_d=180 \text{ days}$$

$$t=180-1= 179 \text{ days}$$

$$K_{td} = \left(\frac{t}{61 - 4f_{ci}' + t} \right) = \frac{178}{61 - 4(6) + 178} = 0.828$$

$$\psi(t_d, t_i) = 1.9 K_{vs} K_{hc} K_f K_{td} t_i^{-0.118}$$

$$\psi(t_d, t_i) = 1.9(0.865)(1)(0.7142)(0.828)(1)^{-0.118} = 0.972$$

Girder creep coefficient at final time due to loading at deck placement

$$t = 20000 - 180 = 19820 \text{ days}$$

$$K_{td} = \left(\frac{t}{61 - 4f_{ci}' + t} \right) = \frac{19820}{61 - 4(6) + 19820} = 0.9981$$

$$\psi(t_f, t_d) = 1.9 K_{vs} K_{hc} K_f K_{td} t_i^{-0.118}$$

$$\psi(t_f, t_d) = 1.9(0.865)(1)(0.7142)(0.9981)(180)^{-0.118} = 0.6348$$

Deck creep coefficients:

Deck creep coefficients at final time due to loading at deck placement

$$V/S = 5$$

$$t = 20000 - 180 = 19820 \text{ days}$$

$$K_{vs} = 1.45 - 0.13(V/S) = 1.45 - 0.13(5) = 0.8 \geq 0.0 \quad o.k$$

$$K_f = \frac{5}{1 + f_c'} = \frac{5}{1 + 4} = 1$$

$$K_{id} = \left(\frac{t}{61 - 4f_{ci}' + t} \right) = \frac{19820}{61 - 4(4) + 19820} = 0.9977$$

$$\psi(t_f, t_d) = 1.9 K_{vs} K_{hc} K_f K_{td} t_i^{-0.118}$$

$$\psi(t_f, t_d) = 1.9(0.8)(1)(1)(0.9977)(180)^{-0.118} = 0.8217$$

Transformed section coefficients for time period between transfer and deck placement:

$$e_{pg} = 20 \text{ in}$$

$$K_{id} = \frac{1}{1 + \frac{E_p}{E_{ci}} \frac{A_{ps}}{A_g} \left(1 + \frac{A_g e_{pg}^2}{I_g} \right) (1 + 0.7 \psi_b(t_f, t_i))}$$

$$K_{id} = \frac{1}{1 + \frac{28500}{4463} \frac{5.202}{788.4} \left(1 + \frac{788.4 * 20^2}{260403} \right) (1 + 0.7 * 1.1715)} = 0.855$$

Transformed section coefficients for time period between deck placement and final time:

$$e_{pc} = 36.24 - 4.75 = 31.49 \text{ in}$$

$$K_{df} = \frac{1}{1 + \frac{E_p}{E_{ci}} \frac{A_{ps}}{A_c} \left(1 + \frac{A_c e_{pc}^2}{I_c} \right) (1 + 0.7 \psi_b(t_f, t_i))}$$

$$K_{df} = \frac{1}{1 + \frac{28500}{4463} \frac{5.202}{1214.4} \left(1 + \frac{1214.4 * 31.49^2}{558727} \right) (1 + 0.7 * 1.1715)} = 0.8642$$

Elastic shortening: AASHTO (5.9.5.2.3a)

For the first iteration, calculate f_{cgp} using a stress in the prestressing steel equal to 0.9 of the stress just before transfer.

$$P_t = (0.9)(202.5)(5.202) = 948 \text{ k}$$

$$M_{beam} = \frac{0.821 * 120^2}{8} * 12 = 17736 \text{ k.in}$$

$$f_{cgp} = \frac{P_t}{A} + \frac{(P_t e)y}{I} + \frac{M_{beam}y}{I}$$

$$f_{cgp} = \frac{948}{788.4} + \frac{(948 * (-20))(-20)}{260403} + \frac{17736 * (-20)}{260403} = 1.29 \text{ ksi}$$

$$\Delta f_{pES} = \frac{E_p}{E_{ci}} f_{cgp}$$

$$\Delta f_{pES} = \frac{28500}{4463} * 1.29 = 8.23 \text{ ksi}$$

$$f_{pt} = 202.5 - 8.23 = 194.27 \text{ ksi}$$

For the second iteration, calculate f_{cgp} using a stress in the prestressing steel of 194.27 ksi

$$P_t = (194.27)(5.202) = 1010.6 \text{ k}$$

$$f_{cgp} = \frac{1010.6}{788.4} + \frac{(1010.6 * (-20))(-20)}{260403} + \frac{17736 * (-20)}{260403} = 1.472 \text{ ksi}$$

$$\Delta f_{pES} = \frac{28500}{4463} * 1.472 = 9.4ksi$$

$$f_{pt} = 202.5 - 9.4 = 193.1ksi$$

$$Pt = (193.1)(5.202) = 1004.5 \text{ k}$$

$$f_{cgp} = \frac{1004.5}{788.4} + \frac{(1004.5 * (-20))(-20)}{260403} + \frac{17736 * (-20)}{260403} = 1.455ksi$$

$$\Delta f_{pES} = \frac{28500}{4463} * 1.455 = 9.291ksi$$

$$f_{pt} = 202.5 - 9.291 = 193.2ksi$$

$$Pt = (193.2)(5.202) = 1005.02 \text{ k}$$

$$f_{cgp} = \frac{1005.02}{788.4} + \frac{(1005.02 * (-20))(-20)}{260403} + \frac{17736 * (-20)}{260403} = 1.456ksi$$

$$\Delta f_{pES} = \frac{28500}{4463} * 1.456 = 9.3ksi$$

$$f_{pt} = 202.5 - 9.3 = 193.2ksi$$

$$Pt = (193.2)(5.202) = 1005.02 \text{ k}$$

$$f_{cgp} = \frac{1005.02}{788.4} + \frac{(1005.02 * (-20))(-20)}{260403} + \frac{17736 * (-20)}{260403} = 1.456ksi$$

$$\Delta f_{pES} = \frac{28500}{4463} * 1.456 = 9.3ksi$$

Losses: time of transfer to time of deck placement

Shrinkage of girder concrete, (5.9.5.4.2a)

$$K_{hs} = 2 - 0.014H = 2 - 0.014 * 70 = 1.02$$

$$\varepsilon_{bid} = K_{vs} K_{hs} K_f K_{td} * 0.48 * 10^{-3}$$

$$\varepsilon_{bid} = 0.8 * 1.02 * 0.9977 * 1 * 0.48 * 10^{-3} = 0.00039 \quad in/in$$

$$\Delta f_{pSR} = \varepsilon_{bid} E_p K_{id} = 0.00039 * 28500 * 0.8642 = 9.6 ksi$$

Creep of girder concrete AASHTO (5.9.5.4.2b)

$$\Delta f_{pCR} = \frac{E_p}{E_{ci}} f_{cgp} \psi_b(t_d, t_i) K_{id}$$

$$\Delta f_{pCR} = \frac{28500}{4463} 1.456 * 0.972 * 0.8642 = 7.81 ksi$$

The relaxation loss Δf_{pRI} may be assumed equal to 1.2 ksi for low-relaxation strands.

Losses: time of deck placement to final time.

Shrinkage of girder concrete AASHTO (5.9.5.4.3a)

$$\varepsilon_{bif} = K_{vs} K_{hs} K_f K_{td} * 0.48 * 10^{-3}$$

$$\varepsilon_{bid} = 0.8 * 1.02 * 0.9977 * 0.9981 * 0.48 * 10^{-3} = 0.00039 \quad in / in$$

$$\varepsilon_{bdf} = \varepsilon_{bif} - \varepsilon_{bid} = 0.00039 - 0.00039 = 0$$

$$\Delta f_{pSD} = \varepsilon_{bdf} E_p K_{df} = 0$$

Creep of girder concrete AASHTO (5.9.5.4.3b)

$$\Delta f_{cd} = -\frac{M_{slab} y}{I} - \frac{(M_{barrier} + M_{FWS}) y_{comp}}{I_{comp}}$$

$$\Delta f_{cd} = -\frac{945 * 12 * (-20)}{260403} - \frac{(102.6 + 128.5) 12 * (-31.49)}{558727} = 1.03 ksi$$

$$\Delta f_{pCD} = \frac{E_p}{E_{ci}} f_{cgp} (\psi_b(t_f, t_i) - \psi_b(t_d, t_i)) K_{df} + \frac{E_p}{E_c} \Delta f_{cd} \psi_b(t_f, t_d) K_{df} \geq 0$$

$$\begin{aligned} \Delta f_{pCD} &= \frac{28500}{4463} 1.456 (1.1715 - 0.972) 0.8642 \\ &+ \frac{28500}{4821} 1.03 * 0.8217 * 0.8642 \end{aligned}$$

$$\Delta f_{pCD} = 5.92 ksi$$

Shrinkage of deck concrete AASHTO (5.9.5.4.3c)

Strain due to shrinkage

$$\varepsilon_{ddf} = K_{vs} K_{hs} K_f K_{td} * 0.48 * 10^{-3}$$

$$\varepsilon_{ddf} = 0.865 * 1.02 * 0.9977 * 0.9981 * 0.48 * 10^{-3} = 0.000421 \quad in / in$$

$$\Delta f_{cdf} = \frac{\varepsilon_{ddf} A_d E_{cd}}{(1 + 0.7 \psi_d(t_f, t_d))} \left(\frac{1}{A} + \frac{e_{pc} e_d}{I_c} \right)$$

$$\Delta f_{cdf} = \frac{0.000421(504)(4074)}{(1 + 0.7 * 0.8217)} \left(\frac{1}{1214.4} + \frac{31.499(-21.26)}{558727} \right)$$

$$\Delta f_{cdf} = -0.205 ksi$$

$$\Delta f_{pSS} = \frac{E_p}{E_c} \Delta f_{cdf} K_{df} (1 + 0.7 \psi_b(t_f, t_d))$$

$$\Delta f_{pSS} = \frac{28500}{4821} (-0.205) 0.8642 (1 + 0.7 * 0.8217) = -1.65 ksi$$

Total losses:

$$\Delta f_{pLT} = (\Delta f_{pSR} + \Delta f_{pCR} + \Delta f_{pR1})_{id} + (\Delta f_{pSD} + \Delta f_{pCD} + \Delta f_{pR2} + \Delta_{pSS})_{df}$$

$$\Delta f_{pLT} = (9.6 + 7.81 + 1.2) + (0 + 5.92 + 1.2 - 1.65) = 24.08 ksi$$

$$\Delta f_{pT} = \Delta f_{pLT} + \Delta f_{pES} = 24.08 + 9.3 = 33.37 ksi$$

Strand arrangement:

Now that the total loss in the prestressing steel stress has been calculated, check if the preliminary strand pattern and eccentricity are still valid. The calculated effective stress in the prestressing steel is:

$$f_{pe} = 202.5 - 33.38 = 169.12 \text{ ksi}$$

For interior beam

$$P_e = \frac{-0.25 - (-4.16)}{\left(\frac{1}{788.4} - \frac{(-20)}{10521} \right)} = 1233.7 \text{ k}$$

$$(169.12)(0.217) = 36.7 \text{ k}$$

The number of strands required

$$\frac{1233.7}{36.7} = 33.6$$

The preliminary strand arrangement with 34 strands is still good.

Service limit state:

Calculate the beam stress limits for two conditions: temporary before losses for the release condition and after all losses for the service condition. For the temporary before losses condition (5.9.4.1):

Tension:

$$0.0948\sqrt{f'_c} = 0.0948\sqrt{6} = 0.232ksi > 0.2ksi \quad use 0.2ksi$$

Compression:

$$0.6f'_c = 0.6 * 6 = 3.6ksi$$

At all service limit state after all losses (5.9.4.2)

Tension: severe corrosion condition:

$$0.0948\sqrt{f'_c} = 0.0948\sqrt{7} = 0.25ksi$$

Compression:

Due to effective prestress and permanent loads:

$$0.45f'_c = 0.45 * 7 = 3.15ksi$$

Due to live load and one-half the sum of effective prestress and permanent loads:

$$0.4f'_c = 0.4 * 7 = 2.8ksi$$

Due to effective prestress, permanent loads, and transient loads:

$$0.6\phi_w f'_c$$

The reduction factor ϕ_w is equal to (1) if the flange slenderness ratio is not greater than

15. The slenderness ratio is the ratio of the flange width to depth:

$$\frac{\text{flange}}{\text{flange}} \frac{\text{width}}{\text{depth}} = \frac{72}{7} = 10.28$$

Since this value is not greater than 15, ϕ_w is equal to (1) and the stress limit is:

$$0.6\phi_w f'_c = 0.6 * 1 * 7 = 4.2ksi$$

The stress limits for the concrete deck slab at the service limit state:

Compression:

Due to effective prestress and permanent loads:

$$0.45f'_c = 0.45 * 4 = 1.8ksi$$

Due to effective prestress and permanent loads, and transient loads:

$$0.6\phi_w f'_c = 0.6 * 1 * 4 = 2.4ksi$$

The total area of prestressing steel, the initial or transfer prestressing force, and the effective prestressing force are:

$$A_{ps} = 0.217 * 34 = 7.378in^2$$

$$P_t = (f_{pt})(A_{ps}) = (193.2)(7.378) = 1425.4k$$

$$P_e = (f_{pe})(A_{ps}) = (169.13)(7.378) = 1247.84k$$

Stresses at transfer:

$$f_{bottom} = \frac{P_t}{A} - \frac{(P_t e)y}{I} - \frac{M_{beam}y}{I} \quad (\text{Service I limit state})$$

$$f_{top} = \frac{P_t}{A} + \frac{(P_t e)y}{I} + \frac{M_{beam}y}{I} \quad (\text{Service I limit state})$$

At the harp point due to the initial prestress force and the beam dead load

$$M_{beam} = 1438.4 * 12 = 17260.7k.in$$

$$f_{bottom} = \frac{1425}{788.44} - \frac{(1425)(-20)(24.751)}{260403} - \frac{17260(24.751)}{260403} = 2.8ksi(c)$$

$$f_{top} = \frac{1425}{788.44} + \frac{(1425)(-20)(29.249)}{260403} + \frac{17260(29.249)}{260403} = 0.54ksi(c)$$

At the ends of transfer length due to the initial prestress force and the beam dead load:

The transfer length is 60 strand diameter or 36 inches. Therefore, the end of the transfer length is 36 inches from the end of the beam or 30 inches from the centerline of bearing, the 0.0208 point. The eccentricity of the prestressing force is:

$$e=8.3 \text{ in}$$

$$M_{beam} = 120 * 12 = 1440 k.in$$

$$f_{bottom} = \frac{1425}{788.44} - \frac{(1425)(-8.3)(24.751)}{260403} - \frac{1440(24.751)}{260403} = 2.79 ksi(c)$$

$$f_{top} = \frac{1425}{788.44} + \frac{(1425)(-8.3)(24.751)}{260403} + \frac{1440(24.751)}{260403} = 0.82 ksi(c)$$

Stresses at service condition:

The service stresses, assuming tension at the bottom fibers, can be calculated using:

$$f_{bottom} = \frac{P_e}{A} - \frac{(P_e e)y}{I} - \frac{(M_{beam} + M_{slab})y}{I} - \frac{(M_{barrier} + M_{FWS} + 0.8M_{LL})y}{I_c} \text{ (Service III limit state)}$$

$$f_{top} = \frac{P_e}{A} + \frac{(P_e e)y}{I} + \frac{(M_{beam} + M_{slab})y}{I} + \frac{(M_{barrier} + M_{FWS} + M_{LL})y}{I_c} \text{ (Service I limit state)}$$

Interior beam:

At end of transfer length due to the effective prestress force and dead load:

$$f_{bottom} = \frac{1247.8}{788.44} - \frac{(1247.8)(-8.3)24.751}{260403} - \frac{(1440 + 924.5)24.751}{260403} - \frac{(100.3 + 125.7)36.24}{558727} = 2.32 ksi$$

$$f_{top} = \frac{1247.8}{788.44} + \frac{(1247.8)(-8.3)29.249}{260403} + \frac{(1440 + 924.5)29.249}{260403} + \frac{(100.3 + 125.7)17.76}{558727} = 0.756ksi$$

At mid span due to the effective prestress force and dead load:

$$f_{bottom} = \frac{1247.8}{788.44} - \frac{(1247.8)(-20)24.751}{260403} - \frac{(1478 + 945)12 * 24.751}{260403} - \frac{(102.6 + 128.5)12 * 36.24}{558727} = 1.01ksi(c)$$

$$f_{top} = \frac{1247.8}{788.44} + \frac{(1247.8)(-20)29.249}{260403} + \frac{(1478 + 945)12 * 29.249}{260403} + \frac{(102.6 + 128.5)12 * 17.76}{558727} = 2.13ksi(c)$$

At mid span due to the effective prestress force, dead load, and live load :

$$M_{LL+I} = 1952k.ft$$

$$f_{bottom} = \frac{1247.8}{788.44} - \frac{(1247.8)(-20)24.751}{260403} - \frac{(1478 + 945)12 * 24.751}{260403} - \frac{(102.6 + 128.5 + 0.8 * 1952)12 * 36.24}{558727} = -0.2ksi(t)$$

$$f_{top} = \frac{1247.8}{788.44} + \frac{(1247.8)(-20)29.249}{260403} + \frac{(1478 + 945)12 * 29.249}{260403} + \frac{(102.6 + 128.5 + 1952)12 * 17.76}{558727} = 2.87ksi(c)$$

At mid span due to live load and one-half the effective prestress force and dead load

$$f_{top} = \frac{1}{2} \left(\frac{1247.8}{788.44} + \frac{(1247.8)(-20)29.249}{260403} + \frac{(1478 + 945)12 * 29.249}{260403} \right. \\ \left. + \frac{(102.6 + 128.5)12 * 17.76}{558727} \right) + \frac{1952 * 12 * 17.76}{558727} = 1.81 \text{ksi}(c)$$

Strength limits state:

The strength limits state includes checks on the nominal flexural resistance and the amount of prestressed reinforcement. For practical design the rectangular stress distribution can be used.

Nominal flexural resistance- mid span:

1-The factored moments for the strength I limit state, Mu is:-

$$M_u = 1.25(1478 + 945 + 102.6) + 1.5(128.5) + 1.75(1952) = 6765.75 \text{k.ft}$$

1- Calculate the depth of the compression block (5.7.3.1.1)

$$b = 72 \text{ in}$$

$$d_p = 7 + 54 - 4.75 = 56.25 \text{ in}$$

$$K = 0.28$$

$$\beta_1 = 0.85 \text{ for } f'_c = 4 \text{ ksi deck concrete}$$

In order to calculate the depth of the compression block, a, first calculate the depth to the neutral axis, c, assuming rectangular section behavior.

$$c = \frac{A_{ps}f_{pu} + A_s f_y - A'_s f'_y}{0.85 f'_c \beta_1 b + k A_{ps} \frac{f_{pu}}{d_p}}$$

$$c = \frac{7.378 * 270 + 0 - 0}{0.85(4)(0.85)(72) + 0.28(7.378) \frac{270}{56.25}} = 9.1in$$

Since the depth to the neutral axis is larger than the slab thickness, the assumed rectangular section behavior is incorrect. We have to calculate the new (c) assuming T-section:

$$c = \frac{A_{ps}f_{pu} + A_s f_y - A'_s f'_y - 0.85 f'_c (b - b_w) h_f}{0.85 f'_c \beta_1 b_w + k A_{ps} \frac{f_{pu}}{d_p}}$$

$$c = \frac{7.378 * 270 + 0 - 0 - 0.85(4)(72 - 20)7}{0.85(4)(0.85)(20) + 0.28(7.378) \frac{270}{56.25}} = 11.14in$$

3-Calculate the stress in the prestressing steel at the nominal flexural resistance
(5.7.3.1.1)

$$f_{ps} = f_{pu} \left(1 - k \frac{c}{d_p} \right)$$

$$f_{ps} = 270 \left(1 - 0.28 \frac{11.14}{56.25} \right) = 255ksi$$

4-Calculate the factor flexural resistance (5.7.3.2.2-1)

$$\begin{aligned}
 M_n &= A_{ps}f_{ps} \left(d_p - \frac{a}{2} \right) + A_s f_s \left(d_s - \frac{a}{2} \right) - A'_s f'_s \left(d'_s - \frac{a}{2} \right) \\
 &+ 0.85 f'_c (b - b_w) h_f \left(\frac{a}{2} - \frac{h_f}{2} \right) \\
 M_n &= (7.378 * 255) \left(56.25 - \frac{11.14}{2} \right) + 0 \\
 &+ 0.85(4)(72 - 20)(7) \left(\frac{11.14}{2} - \frac{7}{2} \right) / 12 = 8159.2k.ft
 \end{aligned}$$

$$M_r = \phi M_n = (1)(8159) = 8159k.ft > 6765.75k.ft$$

O.K

Reinforcement limits-mid span:

Check the reinforcement limits, maximum and minimum. The maximum amount of prestressed and non-prestressed reinforcement (5.7.3.3.1) should satisfy:

$$\frac{c}{d_e} \leq 0.42$$

$$d_e = \frac{A_{ps}f_{ps}d_p + A_s f_y d_s}{A_{ps}f_{ps} + A_s f_y} = \frac{7.378 * 255 * 56.25 + 0}{7.378 * 255} = 56.25in$$

$$\frac{c}{d_e} = \frac{11.14}{56.25} = .2 \leq 0.42 \quad O.K$$

The minimum amount of prestressed and non-prestressed reinforcement is the amount needed to develop a factored resistance, M_r , equal to the lesser of the following (5.7.3.3.2):

$$1.2M_{cr}$$

$$1.33 \text{ times the factored moments (strength limit state, } M_u)$$

The cracking moment, M_{cr} , may be taken as:

$$M_{cr} = S_c (f_r + f_{cpe}) - M_{dnc} \left(\frac{S_c}{S_{nc}} - 1 \right) \leq S_c f_r$$

$$f_r = 0.24 \sqrt{f'_c} = 0.42 \sqrt{7} = 0.635 \text{ ksi}$$

$$f_{cpe} = \frac{1247.8}{788.44} + \frac{1247.8 * 20 * 24.751}{260403} = 3.95 \text{ ksi}$$

$$M_{dnc} = 1478 + 945 = 2423 \text{ k.ft} * 12 = 29076 \text{ k.in}$$

$$S_c = \frac{558727}{36.24} = 15417 \text{ in}^3$$

$$S_{nc} = \frac{260403}{24.751} = 10521 \text{ in}^3$$

$$M_{cr} = (15417(0.635 + 3.95) - 29076 \left(\frac{15417}{10521} - 1 \right)) \frac{1}{12}$$

$$M_{cr} = 4763 \text{ k.ft}$$

$$M_{cr} = 4763 S_c f_r = 15417 * 0.635 / 12 = 815.8 \text{ k.tf}$$

Since, M_{cr} is to be less than or equal to Sc_{fr}

$$1.2M_{cr} = 1.2 * 815.8 = 979 \text{ k.ft}$$

$$1.33M_u = 1.33 * 6765.75 = 8998.4 \text{ k.ft}$$

The lesser of these two values is (979 k. ft) and the factored resistance is 8159 k.ft > 979 k.ft O.K

Chapter Seven

Design of Repair System for Damaged Prestressed Girders Using Fiber Reinforced Polymer (FRP)

7.1 Background

The prestressed adjacent box beams of the bridge carrying NJ Route 35 over the US Route 440 connector are severely deteriorated due to water ingress. Beams number 4 (BM4) and 18 (BM18) on span 1 and span 4 exhibited longitudinal and transverse cracks, large spalls, heavy efflorescence, unsound concrete, leakage and water stains along the beam joints and bottom of the beams. The visual inspection indicated that the underside of beams BM 4 and BM 18 of both spans had been previously repaired with concrete patch. However, patching appears to have covered the joint between beams, thus water collected and new large spalls resulted, exposing strands at the bottom of beams BM 4 and BM 18. The condition is especially worse in beam BM 18 of span 4 (46.7 ft. long). The spall area is about one quarter of its span. On the bridge deck surface, the asphalt overlay exhibited several wide transverse/longitudinal cracks and a large pothole. The team suspects that seepage at the gutter line is causing water infiltration between beams BM3 and BM4, and BM18 and BM 19, which is leading to deterioration. See Figure 1 and Figure 2 for images of deteriorated beams in Span 1; and Figure 3 and Figure 4 for images of deteriorated beams in Span 4.



Figure 7.1 - Damaged Beams BM3 and BM 4 in Span 1



Figure 7.2 - Damaged Beams BM18 and BM19 in Span 1



Figure 7.3 - Damaged Beams
BM3 and BM4 in Span 4



Figure 7.4 - Damaged Beams
BM18 and BM19 in Span 4

7.2 Summary of Proposed Repair

It is proposed to repair the damaged beam using Fiber Reinforced Polymer (FRP) using a one layer of unidirectional carbon fabric. A careful surface preparation is needed to assure proper bonding of FRP to generate the required tensile force. Proper preparation of surface and initial repair using epoxy mortar will also allow the use of tendons as regular (non-prestressed) reinforcement. Note that part of the prestress will still be effective, and will add to the beam capacity. It is also proposed to verify the contribution of FRP after installment, during the next 2.5 years at which time the bridge is expected to be replaced using staged construction. During the replacement of bridge, the behavior of (some) the repaired beams and their capability to carry any additional loads during the staging will be evaluated by measuring the maximum tensile strains in FRP. After the

bridge replacement, the repaired beam will be further evaluated for determining the effectiveness of FRP for future design and use of FRP. The strength calculations are for beam in the most deteriorated condition.

7.3 Initial repair using epoxy mortar and surface preparation

Since the deterioration to the beam is minimal, the previous patching could be left undisturbed, or those previously repaired areas could be repaired using epoxy mortar to prepare a flat surface for application of FRP. Use the epoxy mortar recommended by the fiber manufacturer.

Beam should be repaired using the following procedure:

1. Remove loose concrete by chipping or hammering. Use only hand held power tools.
2. Apply a corrosion inhibitor.
3. Apply SikaDur® 30 or approved equal epoxy mortar to cover the strands. Apply using manufacturer recommended practices. Apply sufficient material only to create a smooth, flat surface. Re-constituting the original beam section is not necessary.

7.4 FRP Repair design

The FRP repair shall constitute a layer of SikaWrap® 1200C carbon fiber FRP or approved equal. The following properties were considered in the design:

Typical Data (*Material and curing conditions @ 73°F and 50% R.H.*)

RESULTS MAY DIFFER BASED UPON STATISTICAL
VARIATIONS DEPENDING UPON MIXING METHODS AND
EQUIPMENT, TEMPERATURE,

APPLICATION METHODS, TEST METHODS, ACTUAL SITE
CONDITIONS AND CURING CONDITIONS.

Shelf Life 10 years

Storage Conditions Store dry at 40°-95°F (4°-35°C)

Color Black

Primary Fiber Direction 0° (unidirectional)

Area Weight 36.50 oz/sq.yd (1238 g/m²)

Typical Dry Fiber Properties

Tensile Strength 580,000 psi (4.00 GPa)

Tensile Modulus 35.0 x 10⁶ psi (240 GPa)

Elongation 1.7%

Density 0.065 lb/in³ (1.80 g/cm³)

Normal Fiber Thickness 0.064 in. (1.63 mm)

Cured Laminate Properties with Sikadur 300/Sikadur Hex 300 Epoxy

Properties after standard cure [70°-75°F (21°-24°C) - 5 days and 48
hour post cure at 140°F(60°C)]

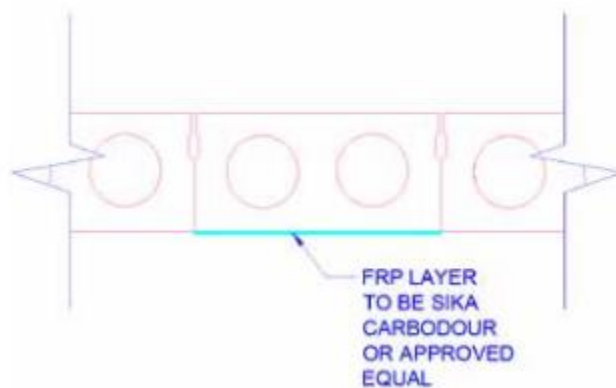


Figure 7.5 - Typical detail of FRP Repair. Beam width is 36-inches. FRP width shall be 30-inches

7.5. A. Repair design calculation

Based on the manufacturers data allowable design strength for the composite ply is 9.9 kips/inch width at a strain level of 0.012. Since FHWA recommendation is to use a maximum FRP strain of 0.005 for ultimate strength computations, a strength value of 4.4 kips/inch width is used for calculations.

Computation of fabric width needed

For the worst case, one beam has 8 strands exposed.

The wire in the beams is 3/8" Dia., 7-wire strands.

The nominal area = 0.080sq.in./strand.

Total area of 8 strands = 0.64 sq. in.

Assuming that all the pre-stress is lost and the strands will act as reinforcement with a stress of 100 ksi when FRP reaches a strain of 0.005 at ultimate load, Tension force needed to compensate for the loss pre-stress = $0.64 \times 150 = 96$ kips

Assuming a force contribution or 4.4 kips/inch width of FRP needed = $96/4.4 = 21.8$ in

Provide a width of 30 in.

Note that, Width of box sections = 36 in.

Therefore, provide one layer of unidirectional carbon fabric that is 30 in, wide.

Check for ultimate load

Since the tensile force capacity of FRP exceeds the capacity lost due to loss of pre-stress, the nominal moment capacity of the repaired beam will be higher than the

original undamaged beam.

Check for working load

Since the moment produced by traffic constitutes a very small fraction of total dead plus live load, the stresses in FRP will be in the order of 10 ksi. This estimate is based on the strain measurements made during the load test conducted in December 2015.

Check for bond

T_{frp} = tensile force per inch width of fabric

(In place as a cured laminate) = 4400 lb (Sika)

$$\Gamma_{int} = 0.065 * (f_c')^{0.5}$$

= $0.065 * 2 = 0.13$ ksi or 130 psi (Assuming the compressive strength of concrete used for the girders is 4000 psi)

B_{frp} = width of the FRP strip = 1 inch

Development length = $4400 / (130 * 1) = 34$ in.

Extend the fabric all the way to the supports. This will provide a bond length of at least 120 in. for the shortest beam.

Check the coupon strength before installation (Quality assurance)

Make coupons during the repair to assure the strength Check bond after repair. The tests will be done only for the fabric chosen for the current repair. Follow manufacturer's recommendations for the preparation of coupons and standard test

protocols (American Concrete Institute committee 440 and FHWA) for testing. The results should be used to verify that the data provided by the manufacturer is achievable.

Non-linear analysis:

The non-linear analysis has been conducted using Desayi model to calculate the maximum strength capacity of the enhanced girders in the bridge. The Desayi model was represented the stress-strain curve in the following equation:

$$f = \frac{E_{\epsilon}}{1 + \left(\frac{\epsilon}{\epsilon_0}\right)^2}$$

An excel sheet was developed to calculate the maximum moment capacity using non-linear approach as shown in (Figure 7.6). The model assumed the enhancement was done using one layer of carbon fiber with 30 inches width, and the maximum strain of FRP equal to 0.005 according to FHWA. The results showed that the capacity of the enhanced section was 898 K.ft; however, the measured moment capacity from the truck test was equal to 470 K.ft, and that provided an adequate margin of safety equal to 1.9.

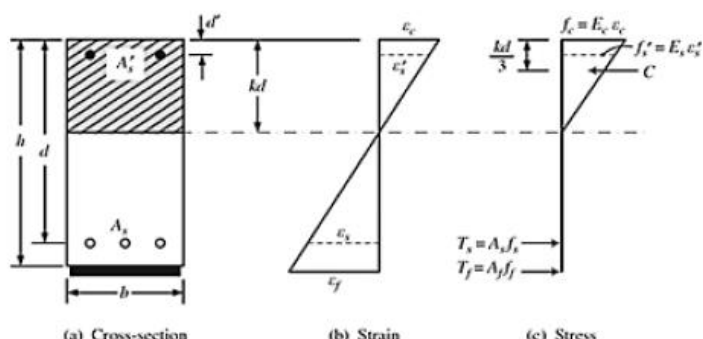
Non-linear analysis of rectangular section with double reinforcement and FRP									
b=	36	in							
h=	27	in							
d=	26	in							
Asp=	2.07	in ²							
fc=	5000	psi							
fy=	100000	psi							
As'=	0	in ²							
d'=	0	in							
εs=	0.00476873	in/in							
εFRP=	0.005	in/in							
FRP width=	30	in							
FRP thick=	0.064	in							
Es=	29000000	psi	Ec=	4030509	psi				
n1=	7.20		EFRP=	24000000	psi				
n2=	5.95								
find the neutral axis from linear elastic behavior (Kd)									
a1=	18								
b1=	26.3267019		$a1(kd)^2 + b1(kd) - c1 = 0$						
c1=	695.927051								
Kd=	5.53	in	neutral axis from linear analysis						
Kd*=	5.38	in	neutral axis from trial and error						
calculate the strain in concrete and β2									
εo=	0.00212132		εc=	0.001244	compression strain in extrem concrete fiber				
εc/εo=	0.58653014		(εc/εo) ² =	0.344018					
β2=	0.5041								
calculate the compression force of the concrete (Cc) kips									
Cc=	439.34	kips							
calculate the tension force of steel (T) kips									
Tmax=	207	kips	tension force at yield point						
Tactual=	286.267021	kips	actual tension force=< tension @yield						
Tuse=	207	kips	smaller of Tmax and Tactual						
calculate the tension force from FRP (TFRP) kips									
TFRP=	230.4	kips							
then calculate the compression force of steel (Ts) kips									
Cs(max)=	0	kips	εs'=	0.001244	in/in	strain in comp. steel			
Cs(actual)=	0.000	kips	fs'=	36.08	ksi				
Cs(used)=	0.000	kips							
calculate the total tension and compression force and compare									
total compression force(Cc+Cs)=	439.344	kips							
total tension force(Tuse+TFRP)	437.400	kips							
check the convergency									
error=	Good	<1%							
K2=	0.3533								
calculate the capacity of the section									
M=	10778.17	k-in	898.18	K.ft					
calculate the stress in compression fiber									
fc=	3.928	ksi							

Figure 7.6 - calculate the maximum moment capacity using non-linear approach

7.5. B. Repair design calculation

If the contribution from damaged prestressed wires is assumed to zero, the area of replaced with carbon area of FRP.

Assuming an average E value of 20×10^6 psi for carbon, area needed for carbon fabric is:

Computation of fabric width needed

For the worst case, one beam has 26 strands exposed.

The wire in the beams is 3/8" Dia., 7-wire strands.

The nominal area = 0.080sq.in./strand.

Total area of 8 strands = 2.08 sq. in.

Assuming that all the pre-stress is lost and the strands will act as reinforcement with a stress of 100 ksi when FRP reaches a strain of 0.005 at ultimate load, Tension force needed to compensate for the loss pre-stress = $2.08 \times 150 = 96$ kips

Assuming a force contribution or 4.4 kips/inch width of FRP needed = $312/4.4 = 70$ in

Provide a width of 35 in, 2 layers.

Note that, Width of box sections = 36 in.

Therefore, provide two layer of unidirectional carbon fabric that is 35 in, wide.

Chapter Eight

CONCLUSIONS

Based on the observations made during the experimental investigation and analytical results the following conclusions can be drawn.

- The truck load test can provide an excellent tool to estimate the residual capacity of the damaged girders and evaluate the response of the bridge elements for applied standards live loads.
- Three different types of test can be performed: statistic test, dynamic test, and crawling test. In addition, there are different types of data can be collect in these tests. A bridge engineer can use this data for (1) improved load rating based on in service data, (2) monitoring bridge performance under permit vehicles, (3) fatigue investigations, and (4) as part of the biannual inspection for improved maintenance of the bridge.
- The Health Monitoring System and other system like it, can be used as a tool by DOT's and bridge engineer to collect quantitative information about the response of the bridges, which can then become part of the permanent bridge maintenance and inspection record. The information can be used for good maintenance and management for the bridges.
- Using commercial carbon fiber reinforced polymer (CFRP) in fabric form is a feasible approach to enhance the capacity of the girders and extend the life time of the bridge, and increasing the CFRP area will increase the strength capacity of the girders, however, there is a limit to use in order to get the maximum capacity, after which increasing the area of CFRP will not be effective.

- One of the most important field observations in this bridge was the way of connecting the girders for each other using shear key. These types of connection was the main reason to get this deterioration in the bridge by preventing water to come through and collecting it, then the steel will tend to corrode.
- The allowable stress in carbon fiber can be decreased by increasing the thickness of the reinforcing layer to keep the strain in the CFRP within the maximum limit suggested by FHWA.
- Using inorganic matrix to provide the required attachment between FRP and the concrete surface is more durable and fire resistant, but have to considering the brittleness of the inorganic matrix.

REFERENCES

- Abe, M., Fujino, Y., Yanagihara, M., & Sato, M. (2000, June). Monitoring of Hakucho Suspension Bridge by ambient vibration measurement. In *SPIE's 5th Annual International Symposium on Nondestructive Evaluation and Health Monitoring of Aging Infrastructure* (pp. 237-244). International Society for Optics and Photonics.
- Chang, Fu-Kuo. *Structural health monitoring 2000*. CRC Press, 1999.
- Campbell Scientific, Inc. 2015 CR6 Measurement and Control System Operator's Manual: Logan, Utah. (PDF version of document downloaded June 05, 2015).
- Çelebi, M., Purvis, R., Hartnagel, B., Gupta, S., Clogston, P., Yen, P., ... & Franke, M. (2004, February). Seismic instrumentation of the Bill emerson memorial mississippi river bridge at cape girardeau (MO): a cooperative effort. In *Proceedings of the 4th International Seismic Highway Conference*.
- Cho, S., Jang, S. A., Jo, H., Mechitov, K., Rice, J. A., Jung, H. J., ... & Seo, J. (2010, March). Structural health monitoring system of a cable-stayed bridge using a dense array of scalable smart sensor network. In *SPIE Smart Structures and Materials+ Nondestructive Evaluation and Health Monitoring*(pp. 764707-764707). International Society for Optics and Photonics.
- Farrar, C. R., & Doebling, S. W. (1997). Lessons learned from applications of vibration based damage identification methods to large bridge structure. *Structural Health Monitoring: Current Status and Perspectives*, 351-370.
- Freyermuth, C. L. (1969). Design of continuous highway bridges with precast, prestressed concrete girders.
- Jang, S., Jo, H., Cho, S., Mechitov, K., Rice, J. A., Sim, S. H., ... & Agha, G. (2010). Structural health monitoring of a cable-stayed bridge using smart sensor technology: deployment and evaluation. *Smart Structures and Systems*, 6(5-6), 439-459.
- Juang, J. N., & Pappa, R. S. (1985). An eigensystem realization algorithm for modal parameter identification and model reduction. *Journal of guidance, control, and dynamics*, 8(5), 620-627.
- Kim, J. T., Ryu, Y. S., Cho, H. M., & Stubbs, N. (2003). Damage identification in beam-type structures: frequency-based method vs mode-shape-based method. *Engineering structures*, 25(1), 57-67.
- Ko, J. M., & Ni, Y. Q. (2005). Technology developments in structural health monitoring of large-scale bridges. *Engineering structures*, 27(12), 1715-1725.
- Mattock, A. H., & Kaar, P. H. (1960). *Precast-Prestressed Concrete Bridges: 3. Further Tests of Continuous Girders*. Portland Cement Association, Research and Development Laboratories.

- Moyo, P., & Brownjohn, J. M. (2002). Application of Box-Jenkins models for assessing the effect of unusual events recorded by structural health monitoring systems. *Structural Health Monitoring*, 1(2), 149-160.
- Pandey, A. K., & Biswas, M. (1994). Damage detection in structures using changes in flexibility. *Journal of sound and vibration*, 169(1), 3-17.
- Balaguru, P., Nanni, A., & Giancaspro, J. (2008). *Frp composites for reinforced and prestressed concrete structures: A guide to fundamentals and design for repair and retrofit*. CRC Press.
- Rice, J. A., & Spencer Jr, B. F. (2009). *Flexible smart sensor framework for autonomous full-scale structural health monitoring*. Newmark Structural Engineering Laboratory. University of Illinois at Urbana-Champaign..
- Soh, C. K., Tseng, K. K., Bhalla, S., & Gupta, A. (2000). Performance of smart piezoceramic patches in health monitoring of a RC bridge. *Smart materials and Structures*, 9(4), 533.
- Sohn, H., Czarnecki, J. A., & Farrar, C. R. (2000). Structural health monitoring using statistical process control. *Journal of Structural Engineering*, 126(11), 1356-1363.
- Structure Number 1223-153, State of New Jersey, New Jersey Department of Transportation data base.
- Todd, M., Johnson, G., Vohra, S., Chen-Chang, C., Danver, B., & Malsawma, L. (1999). Civil infrastructure monitoring with fiber Bragg grating sensor arrays. *Structural Health Monitoring*, 359-368.
- Wong, K. Y. (2004). Instrumentation and health monitoring of cable-supported bridges. *Structural control and health monitoring*, 11(2), 91-124.
- Zimmerman, D. C., & Kaouk, M. (1994). Structural damage detection using a minimum rank update theory. *Journal of Vibration and Acoustics*, 116(2), 222-231.